ISTANBUL TECHNICAL UNIVERSITY ★ GRADUATE SCHOOL OF SCIENCE ENGINEERING AND TECHNOLOGY

AEROELASTIC ANALYSIS OF VARIABLE-SPAN MORPHING WINGS

M. Sc. THESIS

Damla DURMUŞ

Department of Aeronautical and Astronautical Engineering

Aeronautical and Astronautical Engineering Programme

JULY 2020

ISTANBUL TECHNICAL UNIVERSITY ★ GRADUATE SCHOOL OF SCIENCE ENGINEERING AND TECHNOLOGY

AEROELASTIC ANALYSIS OF A VARIABLE-SPAN MORPHING WINGS

M. Sc. THESIS

Damla DURMUŞ
511171107

Department of Aeronautical and Astronautical Engineering

Aeronautical and Astronautical Engineering Programme

Thesis Advisor: Prof. Dr. Metin Orhan KAYA

JULY 2020

İSTANBUL TEKNİK ÜNİVERSİTESİ ★ FEN BİLİMLERİ ENSTİTÜSÜ

KANAT AÇIKLIĞI DEĞİŞTİRİLEBİLEN BİR UÇAK KANADININ AEROELASTİK ANALİZİ

YÜKSEK LİSANS TEZİ

Damla DURMUŞ
511171107

Uçak ve Uzay Mühendisliği Anabilim Dalı

Uçak ve Uzay Mühendisliği Programı

Tez Danışmanı: Prof. Dr. Metin Orhan KAYA

TEMMUZ 2020

Damla Durmuş, a M.Sc. student of ITU Graduate School of Science Engineering and Technology student ID 511171107, successfully defended the thesis/dissertation entitled "AEROELASTIC ANALYSIS OF VARIABLE-SPAN MORPHING WINGS", which she prepared after fulfilling the requirements specified in the associated legislations, before the jury whose signatures are below.

Thesis Advisor :	**Prof. Dr. Metin Orhan KAYA** İstanbul Technical University	....
Jury Members :	**Asst. Prof. Dr. Hayri ACAR** İstanbul Technical University	....
Jury Members :	**Asst. Prof. Dr. Serhat YILMAZ** National Defence University	....

Date of Submission : 15 June 2020
Date of Defense : 14 July 2020

To my family,

FOREWORD

I express my deepest gratitude to my supervisor, Prof. Dr. Metin Orhan Kaya. He has always inspired and encouraged me on the research. I am also thankful to Oğuzhan for his valuable advices, criticism and support throughout this study. Finally, my appreciation are to my family for their endless support and motivation.

July 2020 — Damla DURMUŞ (Aeronautical Engineer)

TABLE OF CONTENTS

Page

ABBREVIATIONS

DTM	: Differential Transformation Method
HALE	: High-Altitude Long-Endurance
LCO	: Limit cycle oscillations
UAV	: Unmanned aerial vehicle
DOF	: Degree of freedom
EA	: Elastic axis
NASA	: National Aeronautics and Space Administration
VCCTEF	: Variable Camber Continuous Trailing-Edge Flap
DARPA	: Defense Advanced Research Projects Agency
MAS	: Morphing Aircraft Structures
AAW	: Active Aeroelastic Wing

SYMBOLS

w	: Plunge deflection
θ	: Pitch deflection
EI	: Bending stiffness
GJ	: Torsional stiffness
m	: Mass of the wing per unit length
ρ_∞	: Air density
I_p	: Polar moment of inertia per unit length
L	: Lift force
M	: Aerodynamic moment
k	: Reduced frequency
U_∞	: Air stream velocity
a	: Elastic axis location
T	: Kinetic energy
U	: Potential energy
X_α	: Static unbalance
R_α	: Radius of gyration
b	: Full span length
c	: Chord length
b	: Semi-chord length
CG	: The center of mass
g	: Artificial damping parameter
ω	: Frequency of motion
V	: Flight speed
I_{EA}	: Mass moment of inertia about elastic axis per unit length
y_0	: Elastic axis position from leading edge

LIST OF TABLES

Page

LIST OF FIGURES

Page

AEROELASTIC ANALYSIS OF A VARIABLE-SPAN MORPHING WINGS

SUMMARY

Aeroelasticity is the field of study that deals with the effects of interaction between aerodynamic, elastic and inertial forces on aircraft structures. Aeroelastic phenomenon may lead to some instability problems such as flutter, divergence and aileron reversal. Flutter is one of the most representative dynamic instability problems of aeroelasticity which may jeopardize the aircraft structure and cause catastrophic failure of an aircraft. The overall safety, flight performance and energy efficiency of an air vehicle are adversely affected by the occurrence of flutter instability condition.

In recent years, there has been an increasing interest to the morphing wing technology due to its capability to perform multi-role missions. In this study, aeroelastic analysis of span morphing concept is analyzed in detail. The telescopic span morphing mechanism has ability to change wing span in order to achieve better aircraft performance, enlarge the flight envelope and accomplish multiple mission roles at different phases of flight. Moreover, asymmetrical wing span extension provides roll control as an alternative to aileron control surfaces. Aeroelastic behavior of span morphing wings are more crucial than conventional wings. Increasing wing span length may cause some dynamic instability problems. For this reason, the flutter characteristics of span morphing wings should be investigated with utmost attention. The motivation behind this study is that making contribution to this growing area by analyzing the flutter behavior of variable-span morphing wings.

This study focuses on the dynamic behavior of variable-span morphing wing oscillating in pitch and plunge motions under subsonic flight conditions. Prior to determining the flutter characteristics of variable-span morphing wing, free vibration and flutter analyses of conventional wing are performed. The unswept cantilevered wing is modeled as an Euler-Bernoulli beam which is widely preferred to simplify the wing structural model. The aerodynamic loads acting on the wing are represented by Theodorsen’s unsteady aerodynamic theory. The governing differential equation of motion that describes the behavior of the dynamics of the Euler-Bernoulli beam is derived through the Hamilton’s principle. The differential transformation method (DTM) is implemented to the governing equations and boundary conditions to obtain the natural frequencies, flutter speed and flutter frequency values. The solution of the aeroelastic system is obtained by the classical frequency domain solution k-method.

To validate the accuracy and reliability of the developed algorithm, Goland wing and a High-Altitude Long-Endurance (HALE) wing are chosen as validation studies. HALE aircraft is equipped with high aspect ratio which causes to more flexible wing, which is an undesirable situation. The wing flexibility leads to geometrical nonlinearities which cause the dynamic instability and decrease in the flutter speed. Therefore, numerous studies related to aeroelastic analysis of HALE wing exist in literature. The free vibration analyses for coupled bending-torsion motion of beam are conducted in both validation cases and compared with the exact values found in

literature. In addition to natural frequencies of the Goland wing and HALE wing, the flutter boundaries of chosen wings are determined. The numerical results are obtained via a script written in MATHEMATICA tool and then compared with the exact solutions of the original Goland and HALE wings. The findings of the numerical analyses presented as quantitatively and qualitatively are in excellent agreement with the exact values found in literature.

The flutter behavior of telescopic span morphing wing oscillating in pitch and plunge motion is investigated. The aircraft wing is modelled as three-stepped Euler-Bernoulli beam. Prior to analyzing the flutter characteristics of morphing wings, numerous validation cases are conducted to ensure that the stepped beam model works well. Goland and HALE wings are also used as the basis for this investigation. The chord lengths of each segment are assumed to be constant along the spanwise. The half span length of wing is the only parameter that changes. By analyzing three-stepped wing models, it is aimed to achieve the same natural frequency with the original Goland and HALE wings which consists of one-segment. After validating the obtained values from analysis of three-stepped beam model, the free vibration and flutter analysis of variable-span morphing wing at 50% span extension is investigated. Furthermore, the flutter speed and flutter frequency is also analyzed for different elongation ratios of wing. There is a significant difference in flutter speeds of fully retracted and fully extended wing configurations. It can be concluded that flutter speed and flutter frequency decreases dramatically as wing span extends. Another important finding is that the flutter speed reduction is relatively high at the initial stages of the wing span extension.

KANAT AÇIKLIĞINI DEĞİŞTİREBİLEN BİR UÇAK KANADIN AEROELASTİK ANALİZİ

ÖZET

Aeroleastisite, hava araçlarının yapısına etki eden aerodinamik, elastik ve ataletsel kuvvetlerin birbiriyle etkileşimini inceleyen çok disiplinli bir bilim dalıdır. Aeroelastisite olgusu statik ve dinamik olmak üzere iki temel kategoride incelenir. Statik aeroelastisitede aerodinamik ve elastik kuvvetlerin etkileşimi incelenirken ataletsel kuvvetler gibi zamana bağlı kuvvetler probleme dahil edilmez. Diverjans gibi statik kararsızlık problemlerinde uçak yapısı üzerinde meydana gelen aerodinamik kuvvetler elastik yapının bozulmasına ve hasar görmesine sebebiyet vermektedir. Dinamik aeroelastisitede ise aerodinamik ve elastik kuvvetlerin yanı sıra zamana bağlı ataletsel kuvvetler de etkileşime dahil olmaktadır. Uçak yapılarında karşılaşılan en önemli dinamik aeroelastik davranışlardan biri çırpınmadır. Hava aracının hızının artışına bağlı olarak aerodinamik sönümleme zamanla azalır ve belirli bir hızda, yapıya etki eden toplam sönümleme değeri sıfırlanır. Böylece hız artışı yapıda bir kararsızlık durumunun oluşmasına sebebiyet verir. Bu noktadan sonra yapıda bir dinamik kararsızlık problemi olan çırpınma, yani kendi kendini besleyen salınımlar, oluşmaktadır. Çırpınma, hava aracının çeşitli yerlerinde görülebilir. Bu çalışmada uçak kanadında meydana gelen kararsızlık problemi incelenmiştir.

Havacılığın ilk yıllarından itibaren hava araçlarında çırpınma problemleri ile karşılaşılmıştır. Tarihte aeroelastik çırpınmadan kaynaklı çokça uçak kazası yaşanmıştır. Uçakların yanı sıra köprü gibi yapılarda da çırpınma kaynaklı yıkımların olduğu görülmüştür. Ölümcül sonuçlara sebep olabilecek bir kararsızlık problemi olmasından dolayı hava aracı tasarımının erken aşamalarında olası çırpınma etkileri ele alınmalıdır. Günümüze kadar uçuş emniyeti ve performansı için son derece önem arz eden çırpınma karakteristiğini analiz edebilmek adına birçok matematiksel ve deneysel model geliştirilmiştir. Ayrıca aeroelastik analizi yapılacak olan bileşenlerin modellenmesi için yapısal ve aerodinamik olarak çeşitli seçenekler mevcuttur.

Şekil değiştirebilen uçaklar farklı isterleri aynı anda elde edebilme amacı taşıyan, son zamanların yenilikçi çalışmalarından biridir. Sabit kanatlı uçaklar, çoğunlukla tek bir görev tanımı için en iyi şekilde tasarlanmaktadırlar. Örneğin avcı uçakları özellikle tırmanış ya da manevra kabiliyeti yüksek olacak şekilde tasarlanmış uçaklardır. Uçuş esnasında şekil değiştirebilme özelliği uçaklara birden fazla görevi yerine getirebilme kabiliyeti kazandırmaktadır. Uçak yapılarının farklı yerlerinde kullanılabilen bu mekanizma, uçuş performansından manevra kabiliyetine, yakıt tasarrufundan daha fazla faydalı yük taşıyabilme özelliğine kadar birçok avantaj sağlayabilir. Şekil değiştirebilme mekanizmasına sahip kanatların aeroelastik davranışı geleneksel kanatlara göre daha kritiktir. Bu nedenle bu yapıların aeroelastik karakteristiğinin incelenmesi son derece önem arz etmektedir.

Bu çalışma kapsamında diferansiyel dönüşüm yöntemi ile şekil değiştirebilen kanat açıklığına sahip bir uçak kanadının ses altı uçuş koşullarındaki aeroelastik

karakteristiği sayısal çözümleme ile incelenmiştir. İlk aşamada uçak kanadı, şekil değiştirme mekanizması dahil edilmeden incelenmiştir. Uçak kanadı, kanat yapısal modelini sadeleştirmek adına yaygın olarak tercih edilen Euler-Bernoulli kirişi olarak modellenmiştir. Kanat üzerine etkiyen değişken aerodinamik yükler için Theodorsen'in aerodinamik teorisi kullanılmıştır. Sayısal çözümleme süresinin uzunluğu bu tür analizlerde karşılaşılabilen problemlerden biridir. Aerodinamik yüklerin Theodorsen'in aerodinamik teorisiyle ifade edilmesi analizi önemli ölçüde sadeleştirmektedir. Bu sebepten dolayı Theodorsen'in aerodinamik teorisi literatürde yaygınca kullanılır. Eğilme ve burulma hareketi yapan Euler-Bernoulli kirişinin enerji ifadeleri verildikten sonra dinamik davranışını tanımlayan hareket denklemleri Hamilton prensibi ile türetilmiştir. Etkili bir çözüm yöntemi olan Diferansiyel Dönüşüm Yöntemi (DDY) tanıtılmış ve hareket denklemleri ile sınır şartlarını yeni ifadelere dönüştürmek için gerekli kurallar verilmiştir. DDY ile Euler-Bernoulli kirişinin hareket denklemleri ve sınır koşulları yeniden ifade edilmiştir. Dönüştürülmüş hareket denklemleri ile sınır koşulları MATHEMATICA yazılımında hazırlanan kod ile çözülmüştür.

Geliştirilen kodun doğruluğunu ve güvenilirliğini teyit etmek amacıyla literatürde çırpınma değerleri mevcut olan Goland kanadı ile HALE kanadı seçilmiştir. HALE uçağı yüksek kanat açıklık oranına sahip tasarımından dolayı bazı kararsızlık durumlarına meyillidir. Kanadın esnek yapısı geometrik doğrusalsızlıklara yol açarak istenmeyen bir şekilde çırpınma hızının düşmesine sebep olur. Bu nedenle HALE kanadının literatürde çokça aeroelastik çalışma örnekleri mevcuttur. Doğrulama çalışmalarında birebir aynı yapısal ve geometrik parametreler kullanılmıştır.

Öncelikle geliştirilen kod yardımıyla dönüştürülmüş denklemlerin çözülmesi ile Goland ve HALE kanatları için farklı modlarda doğal frekans değerleri elde edilmiştir. Aynı kanat modelleri için yapılmış olan serbest titreşim analizlerinden elde edilen doğal frekans değerleri, literatürdeki çalışmalarda her bir mod için elde edilmiş olan değerlerle karşılaştırılmıştır. Aynı zamanda bu karşılaştırma ile farklı yöntemlerin de doğru değere ne derece yaklaşık sonuç verebildiğinin kıyaslanma fırsatı olmuştur. Yapılan çalışmanın literatürdeki verilerle kıyaslaması ile oldukça düşük hata paylarıyla çok yakın sonuçlar elde edildiği görülmüştür.

Eğilme ve burulma hareketi yapan Euler-Bernoulli kirişi olarak modellenen uçak kanadının çırpınma analizleri de Goland ve HALE kanatlarının yapısal ve geometrik özellikleri kullanılarak gerçekleştirilmiştir. Sistemin aeroelastik analizi için klasik aeroelastik çözüm yöntemlerinden biri olan ve literatürde yaygınca kullanılan k-yönteminden yararlanılmıştır. Bu yöntemde, aeroelastik sistemin çırpınma karakteristiğini tanımlayabilmek için yapay sönümleme parametresi kullanılmaktadır. Yararlanılan yapay sönümlemenin ilk kez pozitif değer aldığı yerde çırpınma gözlemlenmektedir. Çırpınma hızı, uçuş hızının sönümleme ile değişimini gösteren grafikten sönümlemenin grafiği kestiği, yani sönümleme değerinin eksiden artıya geçtiği, yerin tespit edilmesiyle bulunmuştur. Aynı şekilde çırpınma frekansı da mevcut çalışmadan elde edilen bir diğer aeroelastik değer olmuştur. Çırpınma frekansı da çırpınma hızının tespit edilmesine benzer bir yöntemle, çırpınma frekansının sönümleme ile değişim grafiğinden bulunmuştur. Benzer şekilde eğrinin ekseni kestiği yer çırpınma frekansını vermektedir. Bulunan çırpınma değerleri literatürde Goland ve HALE kanatlarının aeroelastik analizlerinden elde edilen değerlerle karşılaştırılmıştır. Uçak kanadının doğal frekans değerleri ile çırpınma analizinin düşük hata payı ile başarılı bir şekilde yapıldığı doğrulanmıştır.

Kanat açıklığını değiştirebilen bir uçağın çırpınma karakteristiği birçok farklı senaryo için incelenmiştir. Tezin önceki kısımlarında doğrulama çalışmaları için kullanılan Goland ve HALE kanatları, şekil değiştirebilen kanat analizi çalışmalarında da kullanılmıştır. Öncelikle Goland ve HALE kanatları üç basamaklı kiriş şeklinde modellenmiştir. Üç eşit parçalı kirişin serbest titreşim ve çırpınma analizleri gerçekleştirilmiş ve daha önceden bu çalışmada bulunmuş olan değerlerle kıyaslanmıştır. Elde edilen değerler doğrulandıktan sonra farklı uzunluklara sahip üç parçalı kanat modellerinin doğal frekans ve çırpınma analizleri yapılmış olup literatürde var olan değerlerle karşılaştırılmıştır. Üç parçanın da eşit veter uzunluğuna sahip olduğu varsayılarak kanat açıklığının %50'si oranında uzayabilen bir kanat modelinin doğal frekans ve çırpınma karakteristiği incelenmiş ve yine aynı şekilde literatürdeki verilerle doğrulanmıştır. Sonrasında, kanat açıklığını değiştirebilen bir kanadın çeşitli uzama oranlarındaki çırpınma davranışı incelenmiştir. Şekil değiştirebilme özelliği ile kanat açıklığının artmasının, çırpınma hızını ve çırpınma frekansını önemli bir ölçüde azalttığı görülmüştür. Ayrıca kanadın şekil değiştirmesinin ilk aşamalarında çırpınma hızının ve frekansının daha yüksek oranda azaldığı gözlemlenmiştir.

1. INTRODUCTION

1.1 Motivation Behind the Study

During the recent years, morphing wing technology has gained a great deal of attention in the scientific area due to its high level of adaptability. This technology improves the aircraft performance whilst decreasing structural weight and acoustic noise. It can also accomplish multiple roles at different phases of flight. Aeroelastic behavior of morphing wings are more crucial than conventional wings. Thus, aeroelastic analysis of morphing wings play a vital role. The motivation behind this thesis is that making contribution to this growing area of research by investigating the flutter characteristics of telescopic span morphing wings.

1.2 Background of the Study

Aeroelasticity is the field of study that is concerned with the effects of interactions among aerodynamic, elastic and inertial forces on aircraft structures [1]. Collar's aeroelastic triangle illustrates the aeroelastic interactions of forces [2]. Bisplinghoff et al. [3] recreated the Collar's triangle as shown in Figure 1.1. The elastic behavior of an aircraft structure may cause to the aeroelasticity problem. The stiffness of an aircraft structure can be increased for the purpose of decreasing the aeroelastic effects but higher rigidity may disturb the comfort of the passengers. Actually, structural flexibility itself may not be disadvantageous, but aeroelastic phenomenon is occurred when structural deformations cause additional aerodynamic forces.

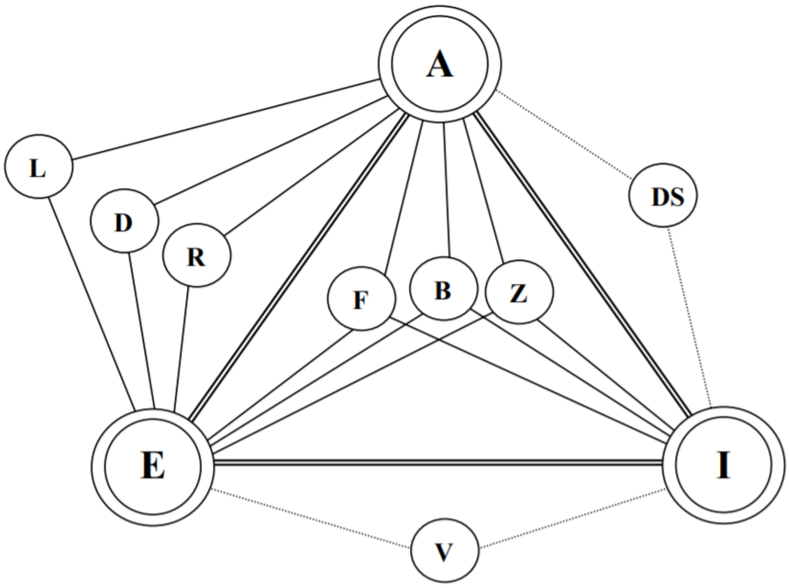

A: Aerodynamic force

E: Elastic force

I: Inertial force

Static Aeroelasticity

L: Load distribution

D: Divergence

R: Control system reversal

Dynamic Aeroelasticity

F: Flutter

B: Buffeting

Z: Dynamic response

Related Fields

V: Mechanical Vibrations

DS: Rigid-body aerodynamic stability

Figure 1.1 : Collar’s Aeroelastic Triangle [3].

Instability conditions that are related to aeroelasticity can be investigated in two main categories which are static and dynamic instability. The categorization of static and dynamic aeroelastic phenomena is illustrated in Table 1.1. The static instability condition is mostly associated with the divergence whilst the dynamic instability condition is mostly associated with the flutter. These phenomena are very crucial since flutter and divergence may cause very harmful results. The divergence has an impact on the structural integrity of an aircraft. It may cause the catastrophic structural failure where the wing theoretically becomes infinite. The flutter is the another stability problem which occurs at a certain speed and frequency which are known as flutter speed and flutter frequency. Flutter instability may be encountered on fixed surfaces, such as the wing, stabilizer or control surfaces. Specialists are required to conduct a flutter-free design in the early stages of the design of an air vehicle.

Table 1.1 : The categorization of static and aeroelastic phenomena.

Static Aeroelastic Phenomena	Dynamic Aeroelastic Phenomena
✓ Divergence	✓ Flutter
✓ Lift Effectiveness	✓ Buffet
✓ Control Surface Effectiveness/Reversal	✓ Limit Cycle Oscillations (LCO)
✓ Aileron Effectiveness/Reversal	✓ Gust Response
	✓ Panel Flutter
	✓ Transient Maneuvers
	✓ Control Surface Buzz

In low speed flights, vibration modes are in steady state which means that flight vehicles return to its steady state condition again after vibration. On the other hand, in high speed flights, these vibration modes may interact with each other. As a result of this interaction, the aircraft may not return to its steady state condition. If the energy cannot dissipate in aircraft structure with damping and friction, vibration modes do not stay at a steady state condition. As flight speed increases from this point, amplitude of vibrations grows and structural damage occurs. Thus, a flight vehicle inclines to undergo potentially destructive aeroelastic motions in high-speed flights [4]. Additionally, aeroelasticity of the hypersonic flight has been a popular subject alongside with the aeroelasticity of subsonic and supersonic flight because of increased needs.

The existence of limit cycle oscillations (LCOs) may cause to unwanted vibrational behavior of airframe and may reduce the vehicle's performance by reducing the cycle fatigue life of the structure. But, since the catastrophic failures can occur abruptly, a more comprehensive insight of complex interaction between the highly flexible structure and the unsteady aerodynamic loading is needed [5].

In recent years, aircraft industry requires multiple mission for the next generation aircrafts. The requirement of achieving high performance prompted the engineers to the morphing wing technologies. There has been an increasing interest in morphing technology from the scientific community through the last decade. The morphing wing technology dates back to studies of Wright Brother. During the recent years, seeking of high-performance conditions caused to back of morphing wing technology to the aircraft industry.

The concept of morphing wing was inspired from the birds who change the shape of their wings to adapt (or perform better) for different flight phases, which can be called as morphing mechanism. The main idea of the morphing wing technology originated from the observation of mechanics and behavior of the birds in flight. Some examples of these morphing behavior of birds includes spanning and sweeping in different flight modes such as diving, flapping, gliding, turning and landing [6]. The birds also can change their winglets by expanding or compressing them in order to alter the velocity.

The morphing wing technology is a feasible way to enhance the flight efficiency, aircraft performance and maneuverability of aircraft while performing several tasks. To gain ability to avoid from stall is another main advantage of the morphing technology.

Morphing concept can be used in several parts of an aircraft and also in other vehicles, such as wind turbine and rotor craft [7].

Materials have a crucial role when designing morphing wing concept. It should be pointed out that it is very important to decide which material is to be used since some of the morphing concepts may increase the weight. Otherwise, the expected advantages may be turn into disadvantages. The materials used in fixed wing aircrafts have very low ductility. Therefore, materials that will be used in the morphing wing should be selected with uttermost attention by considering the type of the mechanism.

The studies conducted on the morphing technology can be associated with the innovative technological discipline of the “smart structures” which can bring real advantages such as increased aerodynamic performance, reduced weight and equivalent safety level [8]. The morphing wing concept is based on the principle that adapt its aerodynamic shape to each flight condition to enhance its performance. This concept can also be categorized in two parts mainly: airfoil-level morphing (2D) and wing-level morphing (3D) [9]. Airfoil-level morphing changes airfoil shape whereas wing-level morphing changes entire shape of the wing. The airfoil shape alteration affects the local aerodynamics which increase the lateral stability and maneuverability. On the other hand, the wing-level morphing changes the twist, sweep, dihedral and span of the wing [9].

Morphing concepts can also be categorized into three main sections which are in-plane morphing, out of plane morphing and airfoil morphing, respectively [10]. Schematic representations of morphing types are categorized and illustrated in Table 1.2.

Table 1.2 : Morphing wing types.

In plane morphing	Out of plane morphing	Airfoil
Sweep	Twist	Camber
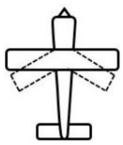	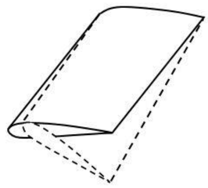	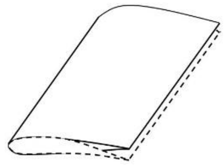
Span	Chord-wise bending	Thickness
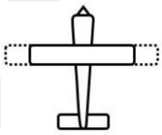	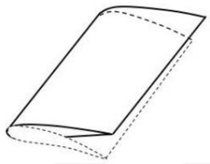	
Chord	Span-wise bending	
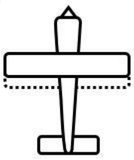	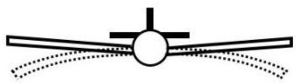	

Another classification can be made according to the morphing level. Folding or variable sweep wing has high morphing level whilst camber morphing has low level.

1.3 History of Aeroelastic Incidents

The first recorded and documented flutter incident was on a Hadley Page's 0/400 twin engine biplane bomber in 1916 in the UK. During a flight the Hadley Page's 0/400 bomber suffered a violent tail oscillation. The coupling of modes of torsion of fuselage and antisymmetric elevator rotation was the main reason behind the accident which was resulted in flutter. Elevators of the aircraft were actuated in an independent way which caused flutter phenomenon [11]. A similar case of flutter occurred in 1917 on the de Havilland DH-9 [12]. During World War I (WWI), a new phenomenon, control surface flutter, was started to present. By means of increasing the control surface's mass balance, this flutter problem was overcomed. On WWI, several catastrophic structural failures on two German fighters, the German Albatros D-III and Fokker D-VII, were identified as aeroelastic static divergence problems [13].

Achieving higher airspeeds and usage of cantilevered wings started to cause wing flutter events after WWI. Primary surface flutter started to show up in 1920s [14]. Air racers experienced several flutter events between the mid-1920s and the mid-1930s. A Curtis R-6 racer developed sudden vibrations caused by wing flutter in 1924. In the following year, Supermarine S-4 Racing Monoplane crashed due to wing flutter [13]. In 1930s, a new flutter type that is called as servo tab flutter which is foreseen that it would be an important problem for many years, started to be investigated. Between 1947 and 1956, eleven cases that include tab flutter were reported for military type aircraft. In 1986, the T-46A trainer aircraft has suffered an aileron flutter during a test flight [11].

In 1947, supersonic speeds were first achieved by Chuck Yeager in X-1 research airplane. Afterwards, flutter at supersonic speeds has become a major research field. Another flutter type, panel flutter, appeared to seem in 1950s due to supersonic speeds. A fighter was disappeared indirectly due to panel flutter.

At that times, control surface and tab buzz problems have emerged for aircraft that fly at transonic speed regime [15]. From 1944 to 1956, twenty-one incidences of flutter are reported including P-80 airplane, F-100 and F-14 fighters.

The all-movable control surface was early suspected as a possible source of flutter difficulties [15]. This suspicion is proven by four incidences from 1953 to 1955.

The carriage of external stores like munitions, fuel tanks and engines affect the aeroelastic stability of an aircraft. From 1947 to 1956, seven incidents of flutter involved the carriage of external stores. Fighters such as F-16, F-18 or F-111 generate a limit cycle oscillation (LCO) that is characterized by sinusoidal oscillations. T-tail flutter, which may be considered similar to the external store problem where the frequencies are relatively low, occurred in 1952 [15]. T-tail flutter effects may be hazardous like flutter due to external stores.

The vertical fin flutter is another flutter problem experienced in history. During a flutter flight test in 1989, vertical fin, rudder and all of the tab of E-6 aircraft were disassembled from the main structure and lost due to flutter [16]. F-117 stealth aircraft also crashed because of flutter that was seen in control rudder, in the United States [17].

The elevon oscillations also may cause the flutter occurrence. In 1997, F-117A Nighthawk experienced large elevon oscillations and these oscillations caused to crash of aircraft while performing a fly-by demonstration for an airshow at Martin State Airport, as shown in Figure 1.2.

Figure 1.2 : F-117A Nighthawk aircraft crash due to elevon-wing flutter [18].

Even though several efforts have been put on developing design flutter tools and software, the most precise method for a flutter-safe design of an aircraft is flight testing. No data was found for the flutter test of a full-scale aircraft regarding the early years of aviation. The methodology of those days was to simply fly the aircraft at its maximum speed to examine the aeroelastic stability characteristics [11]. Flutter tests were also experienced many structural failures. The first known flutter test was conducted in 1935 in Germany by Von Schlippe. Basically, he vibrated the aircraft structures at their natural frequencies for each airspeed and then extracted the resulting amplitudes as illustrated in Figure 1.3 [19].

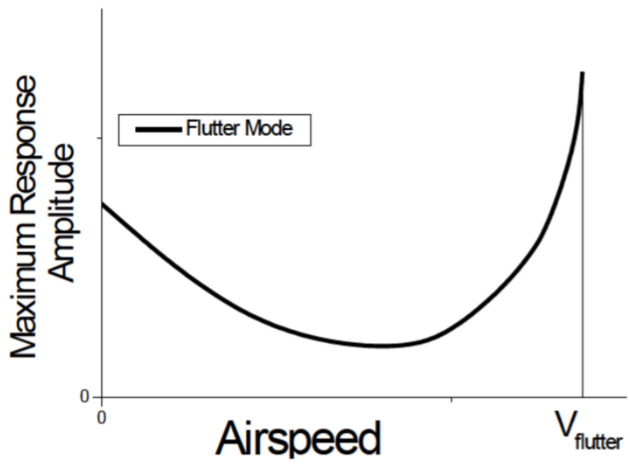

Figure 1.3 : Flight flutter test method of Von Schlippe [19].

This methodology was performed successfully for many German aircraft until a Junker JU90 went into flutter and crashed during flight tests in 1938. Possible reasons of this accident were seen as an improper structural excitation equipment in flight, insufficient response measurement, and incapable recording equipment.

1.4 Literature Survey

This section covers a literature survey of aeroelastic studies from the early days of aeronautics to present. Since 1916 when a flutter incident on Handley Page O/400 twin engine biplane bomber was occurred, flutter phenomenon has attracted the researchers who are dealing with the stability of aircraft wings [13].

Between 1950s and 1970s, several airplanes were installed by excitation systems and accelerometers for sweeping a frequency range to check resonance where damping was manually determined using strip charts [11].

Pioneering studies on the field of aeroelasticity instability of an aircraft dates back to 1920's starting with the study of Frazer & Duncan conducted at National Physical Laboratory, UK. Matrix method and numerical techniques used by them are very common and famous [20]. Hand operated desk calculating machines were used to perform matrix operations. An extensive effort was put in to solve the equation of motion of a semi rigid aircraft employing quasi steady state aerodynamic loads. A disadvantage of the mentioned methodology is that it starts to be inappropriate at high speed regimes. Due to the developments regarding to high-speed flight and low aspect ratio lifting surfaces, the reliability of 2-D unsteady aerodynamic formulation became insufficient in time. The invention of 1st and 2nd generation digital computers made trustworthy solutions of 3-D for subsonic and supersonic regimes possible. A study of Broadbent in 1956 [21] was focused in aeroelastic problems encountered in high-speed flows.

A huge amount of studies in the area of aeroelasticity has been conducted in the United States beginning from the first days of powered flight. A review study performed by Bisplinghoff in 1955 explains both theoretical and experimental approaches to the aeroelasticity phenomenon in detail [3].

With the increase of computational capabilities and reduction in computing costs, numerical methods in structural and fluid mechanics have been developed. Sophisticated and enhanced softwares such as Nastran has been developed and used by researchers world-wide.

Garrick & Reed [13] have a review paper at which they examined the latest developments and current situation in unsteady aerodynamics regarding to the flutter investigations.

Another paper presented by Baldock and Skingle stated that the reduction in flutter and vibration incidents to aircraft indicated that aeroelastic response prediction was sufficiently accurate [22].

In 1968, AGARD has published a user manual in six volumes that is focused on aeroaelasticity problem. On that manual, several contributions from several experts in the field of aeroelasticity were shared along with an enhanced theoretical background of aeroelasticity. Additional extensive surveys and references, dealing with the state of the art in the formulation of the problem, structural modelling, aerodynamic modelling, various phenomena in aeroelasticity and factual information on flutter characteristics and experimental methods were also expressed [23]. For more details, this user manual is highly advised.

Goland [24] examined the flutter behavior of an aircraft wing which is modeled as cantilever beam via integration of the differential equations. It is the classic paper found that a Rayleigh-Ritz type analysis, based on the fundamental uncoupled bending and torsion modes, are entirely adequate for flutter investigations of a uniform wing. Additional parts of the paper dealt with the relation between the uncoupled and the ground modes for the uniform wing, and with the nature of the wing response resulting from forced excitation while in flight [24]. As extended solution of the flutter of uniform wing, Goland and Luke [25] analyzed uniform wing carrying a fuselage and concentrated weights at the tips. They have taken benefit from the Laplace transformation method to solve the differential equations by operational methods for both symmetric and antisymmetric flutter. The main aim was to compare flutter behaviors and speeds for specific uniform wings calculated by the differential equations with the same quantities calculated by the Rayleigh method when only the fundamental bending and torsion modes were used in the calculations [25, 26]. Results of these two methods were found to be sufficiently consistent.

The influence of mounting concentrated weights on the characteristics of flutter are presented experimentally by the Runyan and Sewall [26] for an untapered wing model. There are various analytical techniques to approach the flutter problem for wings when a concentrated weight is of the case. Their findings made it possible to validate the flutter data which are obtained from analytical methods.

Digital computers have had an important role in flight flutter test methods since 1970s. With the help of real time parameter identification methods, phenomena such as damping and frequency are approximated in a Mach number-dependent manner [25].

In 1934, Theodore Theodorsen gave a concise theoretical approach for 2-D oscillating flat plate exposed to basic motions such as translation, torsion and aileron. In his study, he distinguished non-circular and circular parts of the velocity. The trailing edge flow condition sets a relation between the two parts, whose solution leads to a combination of Bessel (or Hankel) functions designated C(k). This relation has been called as Theodorsen’s circulation function C(k) [27].

Throughout the years, the researchers have been developing continuingly the methods for the flutter solution. Lots of hard work were given for the aim of a “true damping” solution of flutter [28]. Subsequent to Theodorsen’s approach to flutter problem, many techniques that aim to identify the stability boundary were developed. It was fairly prevalent to use a parameter that simulated the influence of structural damping [29]. American method, also known as the k-method, is implemented by Smilg and Wessermann [30]. In this method, the problem is solved by introducing an artificial damping parameter. In 1965, Irwin and Guyett developed the p-k method, namely the British method. Unlike the k-method, the pk-method allows complex reduced frequency. It is capable of determining the divergence speed of the system since the value of the reduced frequency can be zero in the solution sequence.

Nonlinear aeroelastic behavior of flight vehicles have been also analyzed by many researchers. In nonlinear flutter, there are sharp changes in speed of flutter as shown in Figure 1.4.

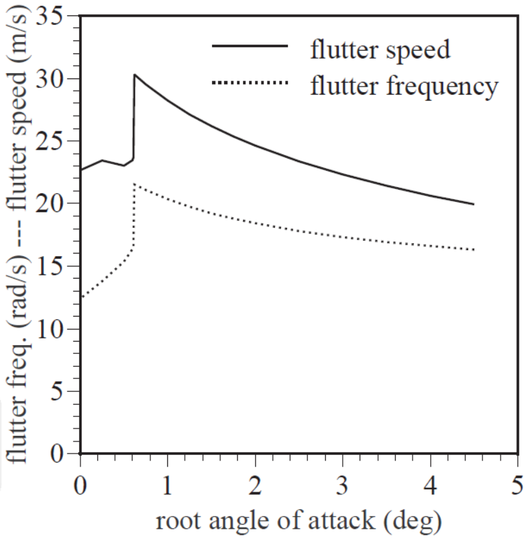

Figure 1.4 : Variation of flutter speed with angle of attack [31].

Recently, Hodges et al. [26-28] have performed an aeroelastic simulation of very light and flexible aircraft for the aim of having next generation of flight vehicles such as UAVs, HALEs and flying wings [32]. Relevant details regarding to HALE aircraft will be introduced in proceeding chapters.

Patil et al. [33] performed a nonlinear aeroelastic analysis of an aircraft in subsonic regime via low-order finite elements. The findings were stated and validated for the Goland wing as shown in Table 1.3. Furthermore, by disregarding the nonlinear trim solution and the flight dynamic frequencies, the estimated aeroelastic characteristic of an aircraft may be unsimilar to the actual result.

Table 1.3: Results for flutter analysis of Goland wing [33].

Method	Flutter velocity, ft/s	Flutter frequency, rad/s
Present analysis	445	70.2
Exact solution	450	70.7
Galerkin solution	445	70.7

The same team in Ref. [33] studied a nonlinear aeroelastic problem and flight dynamics of HALE aircraft, in 2001 [31]. The study found that there exists a powerful relationship between the displacement of wing tip and the speed of flutter, as shown in Figure 1.5.

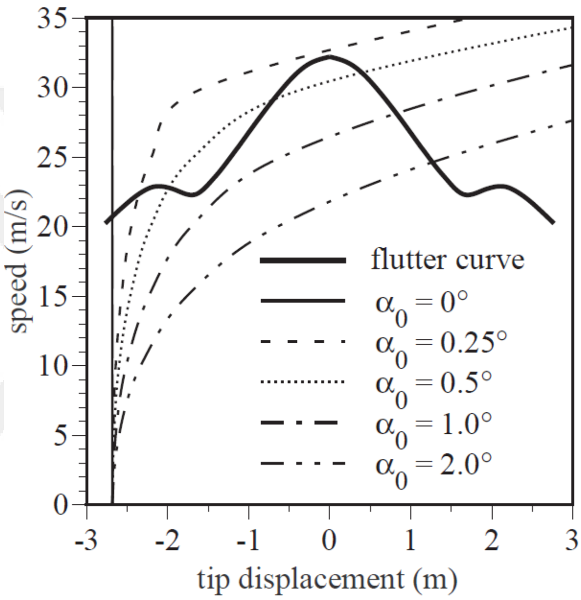

Figure 1.5 : Correlation of speed of flutter and displacement of wing tip [31].

HALE aircraft wing tends to experience enormous deformations in trimmed flight. As a result of these enormous deflections and coupling between the vehicle flight dynamics and wing vibrations, body-freedom flutter occurs. Richards et al. [34] examined the body-freedom flutter behavior of a HALE flying-wing aircraft and sensitivity of this behavior depending on some parameters such as structural coefficients, flange thickness, center of gravity location, fuselage mass factor and fuselage inertia facto. The variation of flutter velocity with inertia factor of fuselage is represented in Figure 1.6.

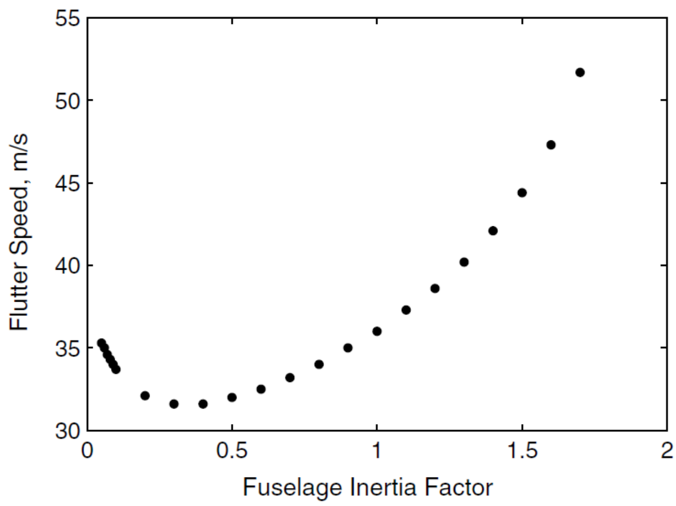

Figure 1.6 : Flutter speed and frequency as a function of a multiplicative fuselage inertia factor [34].

In 2001, Tang and Dowell [35] investigated the aeroelastic behavior of HALE flying-wing aircraft experimentally. A theoretical model has been developed and compared with the experimental data. Figure 1.7a and Figure 1.7b illustrate the comparison of the flutter velocity and frequency obtained from experimental and theoretical data with respect to pitch angle.

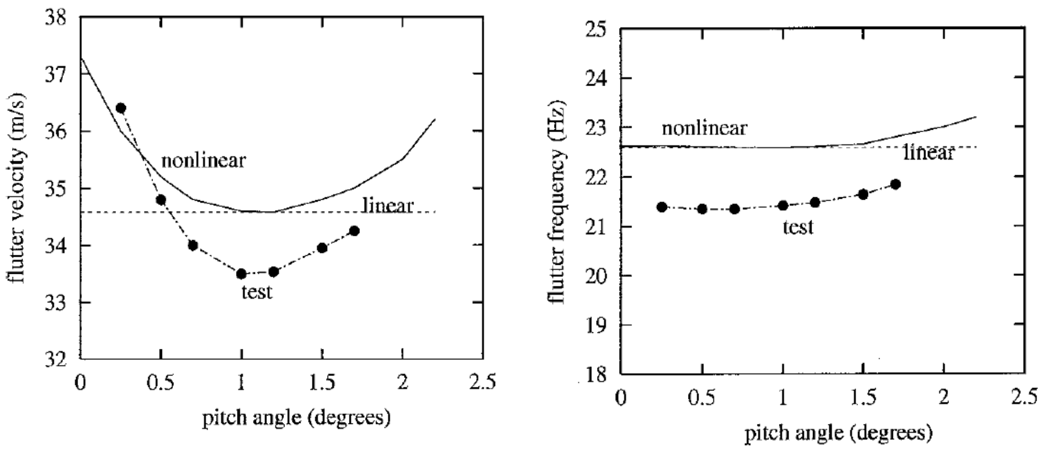

a b

Figure 1.7 : Perturbation eigenvalue solution with respect to pitch angle [35].

In 2004, Moosavi et al. [36] examined the flutter of a linear 3-DOF aeroelastic system using Galerkin method. They pointed out that effects of compressibility when the speed is high subsonic, plays a major role in the flutter speed of wing. Because of the compressibility, a decrease in flutter speed and flutter frequency as compared to the incompressible flow occurs, as shown by Table 1.4. They used the Goland wing for the validation process.

Table 1.4 : Comparison of the calculated flutter results [36].

Method	Description	Flutter speed (Mach)	Flutter frequency (Hz)
Exact	2D incompressible flow	0.554	11.25
Galerkin	2D incompressible flow	0.554	11.15
Galerkin	2D compressible flow	0.526	10.90

The extensive technical background of Goland wing and HALE wing will be given in the related chapters.

Morphing wing concept was studied in aircraft industry since the Wright Brothers. It should be pointed out that the morphing wing technologies studied during last decades is not exactly have same meaning with the work done by Wright Brothers. Morphing changes the shape of a wing in a smooth manner in the current technology, which helps the reduction of drag.

In 1951, the aircraft X-5 has the variable swept wing design which can change its shape depending on speed as shown in Figure 1.8. Then, the same design is used on the aircrafts such as F-14, F-111, Tornado and Dassault Mirage G [10]. Variable swept wing mechanism can increase the lift to drag ratio.

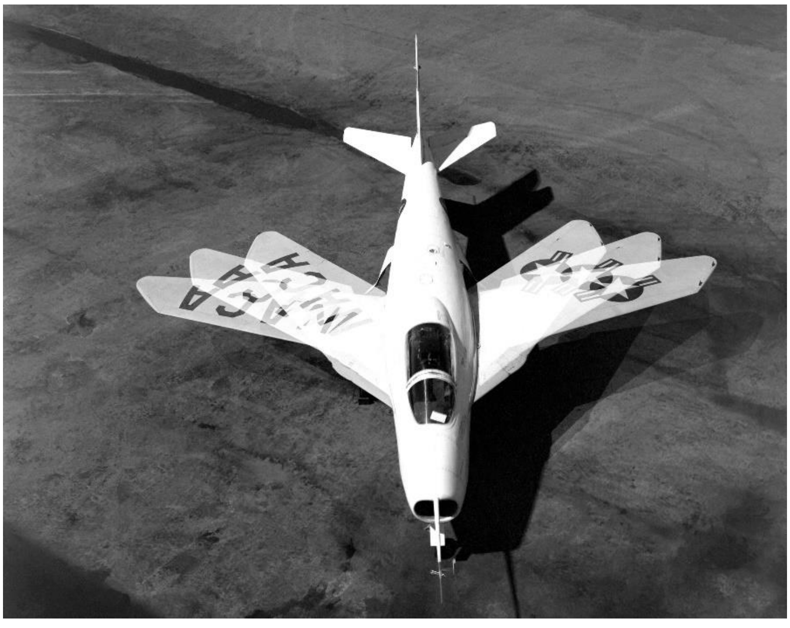

Figure 1.8 : The X-5's variable swept wing capability [10].

Weishuang et al. [37] designed the flexible variable camber trailing-edge flap to enhance the flight performance. They showed that the variable camber trailing-edge flap can increase the lift coefficient by nearly 8% compared with the traditional flap under takeoff configuration and lift-to-drag ratio increased nearly 30% in cruise state. Boeing and NASA jointly presented a Variable Camber Continuous Trailing-Edge Flap (VCCTEF) system which can gain about 10% reduction in cruise drag and loss weight about 9.8% [38]. Another study of morphing concept was carried out by Zi et al. [7] by investigate the aerodynamics characteristics of the morphing wing with a flexible trailing-edge.

Most of the span morphing concept are based on a telescopic mechanism which is introduced by Ivan Mahhonine. In 1931, first known examination of the telescopic span morphing wing was conducted via the Makhonine Mak-10 aircraft. Telescopic wing mechanism enable long endurance flight by extending their wings and reach required distance in very short time.

Blondeau and Pines [39] designed and tested of pneumatic telescopic wing on a UAV which increases the aspect ratio nearly 130%.

In 2003, Defense Advanced Research Projects Agency (DARPA) introduced the Morphing Aircraft Structures (MAS) program to develop morphing capabilities of flight vehicles. The variable span morphing was also investigated in a wind tunnel by Lockheed Martin Aeronautics Company (LM). Figure 1.9 illustrates a test prototype, Lockheed-Martin Agile Hunter, in its morphed and unmorphed configurations. Aeroelastic characteristics are also analyzed during the study but no aeroelastic instabilities were encountered as a direct result of the morphing design [40].

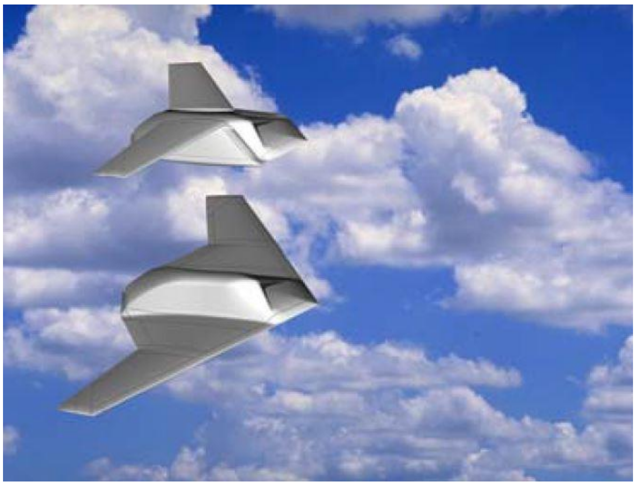

Figure 1.9 : Lockheed-Martin Agile Hunter morphing concept [41].

NASA developed Active Aeroelastic Wing (AAW) program which aims to roll maneuvering control by twisting a flexible wing. The test aircraft was chosen as a modified F/A-18A from U.S. Navy and tests were completed successfully.

Henry and Pines [42] utilized morphing design to achieve roll control. The roll control obtained by morphing mechanism achieves better efficiency compared with the conventional way. They pointed out that the magnitude of damping coefficient increases as the span differential increases.

Seigler et al. [43] also studied asymmetrical wing extension in order to obtain increased maneuverability of bank-to-turn cruise missiles. In addition to increasing the range by span morphing, the roll control can also be obtained by creating moment about the longitudinal axis of the missile. Figure 1.10 illustrates the comparison of the production of roll moment due to asymmetrical wing extension and conventional tail control surfaces.

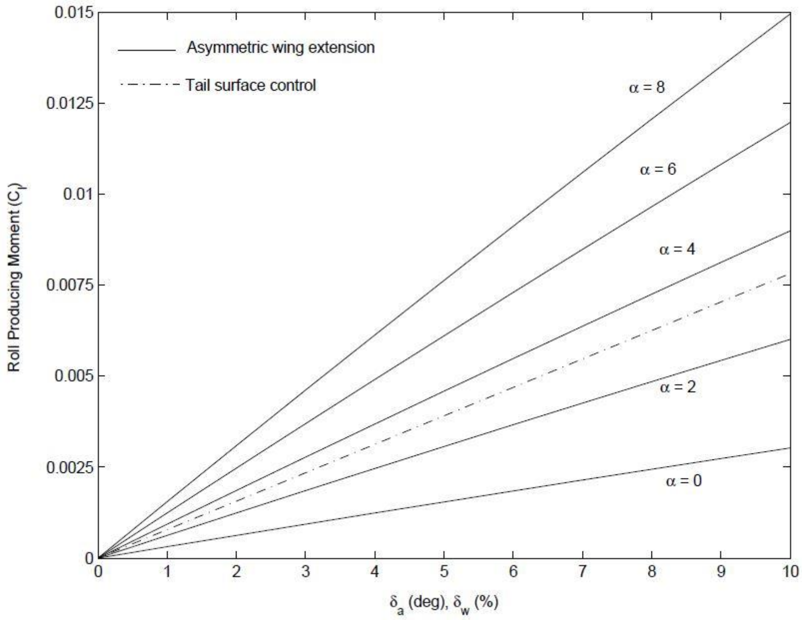

Figure 1.10 : Comparison of the roll producing moment due to asymmetrical wing extension and conventional control surfaces [43].

Ajaj et al. [44] analyzed the span morphing mechanism on endurance capability, induced drag and roll control. They concluded that the better flight efficiency obtained by span morphing. 20% symmetric increase in wing span reduces the drag by 10% at the start of cruise and by 2.5% at the end of cruise.

It should be pointed out that the aeroelastic behavior of morphing wing is more crucial than the aeroelastic behavior of the conventional wing. Li et al. [45] analyzed the nonlinear aeroelastic characteristics of morphing flap and found that the critical flutter speed reduced with existence of morphing mechanism. By performing modal analysis, they were observed a reduction in the values of natural frequencies in the case of wing span was extended.

Huang et al. [46] investigated the significance of rigid-body motions for the flutter mechanism of a span morphing wing. Study deduced that the flutter speed decreases as the wing span increases. They suggested that the rigid-body motions especially the pitch motion should be taken into consideration in the flutter analysis of a span morphing wing to achieve more accurate results.

Huang and Qui [47] analyzed the transient aeroelastic response and flutter of a span morphing wing. One of the important inferences that should be highlighted is the speed of wing extension process. A faster morphing process achieves better aeroelastic performance. As it is well known, the flexibility of the wing increases with the increase of aspect ratio, which is a very essential feature for aeroelastic behavior of a wing. As shown in Figure 1.11, the flutter speed decreases as wing span length increases.

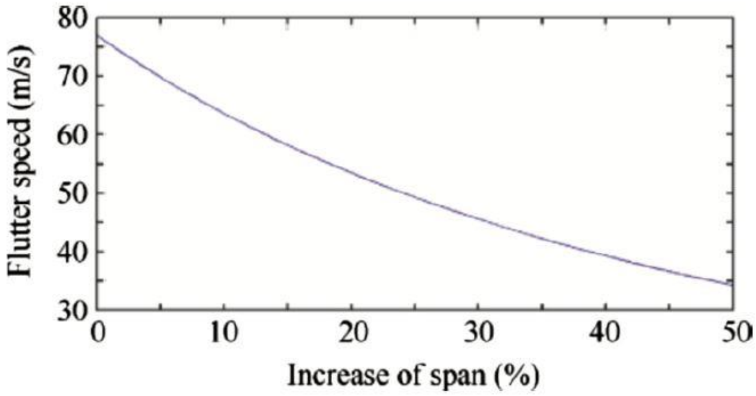

Figure 1.11 : Flutter speed vs. wing span length [47].

1.5 Outline of the Thesis

In this thesis, flutter characteristics of a variable-span morphing wing oscillating in pitch and plunge motions under subsonic flight conditions is analyzed. Brief explanations of the chapters are given in this part. The thesis has been organised in the following way. The overall structure of the thesis takes the form of six chapters. The study begins with a brief overview of the history of aeroelasticity and literature survey about morphing wings in this introductory chapter.

Chapter 2 of this thesis presents the structural and aerodynamic modelling of the aircraft wing. The fundamental technical background of the Euler-Bernoulli beam theory and Theodorsen's unsteady aerodynamic theory are presented. After the energy expressions are stated, the governing differential equation of motion that includes the aerodynamic coefficient are derived by the Hamilton's principle.

Chapter 3 is concerned with the methodology used for this thesis. Firstly, the DTM is briefly introduced. Then, the governing differential equations and the boundary conditions are transformed by the DTM. The k-method, as an aeroelastic solution method, is presented and utilized for the solution of flutter equation.

The findings and discussions of the analyses of aircraft wing are presented in Chapter 4. To validate the accuracy and reliability of the developed algorithm, Goland wing and HALE wing were chosen as validation studies. The results of analyses are discussed as quantitatively and qualitatively.

Chapter 5 presents the investigation of variable-span morphing wing. The wing is modelled as a three-stepped Euler-Bernoulli beam and numerous validation cases are performed. The flutter speed and flutter frequency are analyzed for different elongation ratios of wing. The effects of span extension to the flutter boundaries are also investigated.

Lastly, concluding remarks and observations of the present study are stated and the recommendations for future work are given in Chapter 6.

2. STRUCTURAL AND AERODYNAMIC MODELING

This chapter is devoted to structural and aerodynamic modeling of the cantilevered wing. The cantilevered wing is modeled as an Euler-Bernoulli beam while the aerodynamic loads acting on the wing are represented by Theodorsen's unsteady aerodynamic theory. Then, the equations of motion for free vibration of Euler-Bernoulli beam are derived by Hamilton's principle. After that, the equations of motion that includes the aerodynamic coefficient for aeroelastic flutter are derived.

2.1 Euler-Bernoulli Beam

The Euler-Bernoulli beam theory (also known as classical beam theory) is a widely used method in literature due to its simplicity. It can be easily adapted to represent the dynamics of more complex engineering systems. Especially in aerospace area, the Euler-Bernoulli beam is widely preferred to simplify the wing structural model. Although many sophisticated tools are developed, beam theory still retains its popularity.

The aircraft wing is modeled as a cantilevered Euler-Bernoulli beam where fixed at the root section ($y = 0$) and free at the tip section ($y = l$). The Euler-Bernoulli beam theory has the following kinematic assumptions [48]:

-The material is linear, isotropic and homogenous,

-The cross section of the beam is constant,

-Plane sections of the beam remain plane to the deformed neutral axis (Figure 2.1),

-The cross section of the beam remains plane after deformation,

-The cross section is symmetric in the plane of bending.

Experimental measurements demonstrate that these assumptions are valid for long and slender beams made of isotropic materials with solid cross-sections [48]. When one or more of these conditions are not met, the predictions of Euler-Bernoulli beam theory can become inaccurate.

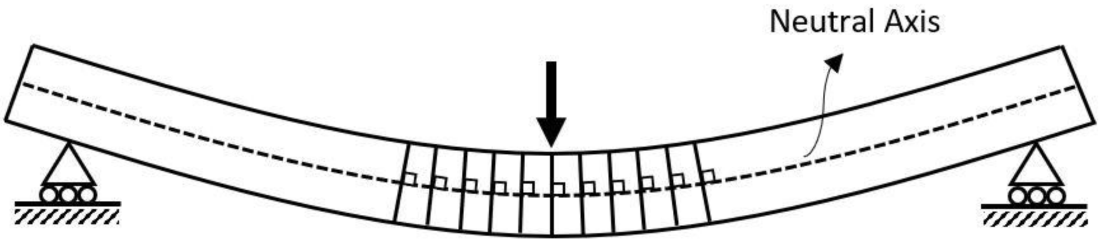

Figure 2.1 : Kinematics of the Euler-Bernoulli beam theory.

The equations of motion of free vibration of a uniform Euler-Bernoulli beam for the bending and torsion are given by

$$EI\frac{\partial^4 w}{\partial y^4} + m\frac{\partial^2 w}{\partial t^2} = 0 \tag{2.1}$$

$$GJ\frac{\partial^2 \theta}{\partial y^2} - \rho I_p\frac{\partial^2 \theta}{\partial t^2} = 0 \tag{2.2}$$

where EI is the bending stiffness, GJ is the torsional stiffess, m is the mass per unit length and I_p is the polar moment of inertia per unit length. The geometric boundary conditions of a uniform cantilevered Euler-Bernoulli beam for bending motion are expressed as following,

Fixed end $(y = 0)$: $$w(0,t) = \frac{\partial w}{\partial y}(0,t) = 0 \tag{2.3}$$

Free end $(y = l)$: $$\frac{\partial^2 w}{\partial y^2}(l,t) = \frac{\partial^3 w}{\partial y^3}(l,t) = 0 \tag{2.4}$$

Similarly, the geometric boundary conditions of a uniform cantilevered Euler-Bernoulli beam for torsion are expressed as following,

Fixed end $(y = 0)$: $$\theta(0,t) = 0 \tag{2.5}$$

Free end $(y = l)$: $$\frac{\partial \theta}{\partial y}(l,t) = 0 \tag{2.6}$$

These are the usual conditions that must be imposed on a vibrating cantilever beam.

2.2 Theodorsen's Aerodynamic Theory

The aerodynamic loads acting on the wing are represented by Theodorsen's unsteady aerodynamic theory. The $C(k)$ is the Theodorsen's function which is a complex-valued function of the reduced frequency. It consists of complex and real parts such that $C(k) = F(k) + iG(k)$ where $F(k)$ represents the real part whilst $G(k)$ represents the imaginary part. Theodorsen's function, also known as a lift deficiency, can only be applied in the case where the response of the system is exactly sinusoidal.

The aerodynamic lift and moment expressions are given in equation 2.7-2.8 in terms of $C(k)$.

$$L = 2\pi\rho_\infty U_\infty bC(k)\left[\dot{w} + U_\infty\theta + b\left(\frac{1}{2} - a\right)\dot{\theta}\right] + \pi\rho_\infty b^2\left(\ddot{w} + U_\infty\dot{\theta} - ba\ddot{\theta}\right) \tag{2.7}$$

$$M = b\left(\frac{1}{2} + a\right)\left\{2\pi\rho_\infty U_\infty bC(k)\left[\dot{w} + U_\infty\theta + b\left(\frac{1}{2} - a\right)\dot{\theta}\right] + \pi\rho_\infty b^2\left(\ddot{w} + U_\infty\dot{\theta} - ba\ddot{\theta}\right)\right\} - \pi\rho_\infty b^3\left[\frac{1}{2}\ddot{w} + U_\infty\dot{\theta} + b\left(\frac{1}{8} - \frac{a}{2}\right)\ddot{\theta}\right] \tag{2.8}$$

where ρ_∞ is the air density, b is the semi-chord length, U_∞ is air stream velocity and a is the elastic axis location.

2.3 The Kinematics of the Wing

The kinematics of the wing is given by the bending deflection (plunge deflection) $w(y,t)$ in the z direction and the torsion rotation (pitch deflection) $\theta(y,t)$ about the elastic axis which may defined as the line of effective shear center. The displacement w and θ of the elastic axis are functions of y and t. For a wing oscillating in bending and torsion in a free stream of fluid, the bending deflection of the elastic axis and the rotation of the wing cross section are illustrated in Figure 2.2.

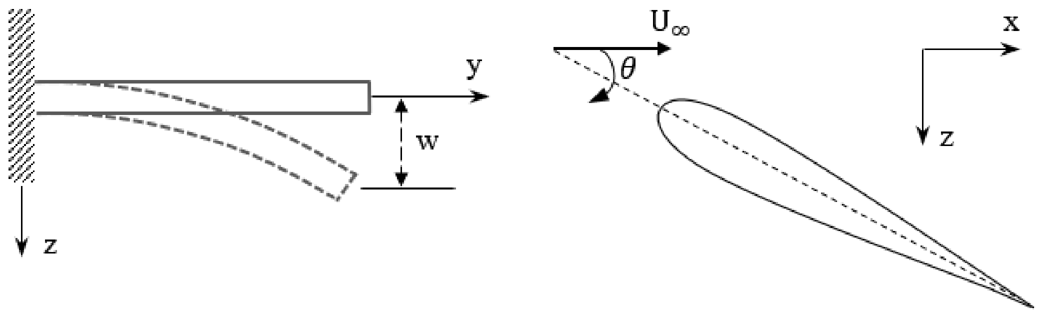

(a) **(b)**

Figure 2.2 : Schematic representation of the (a) wing deflection and (b) rotation.

Another representation of the wing kinematics is given in Figure 2.3.

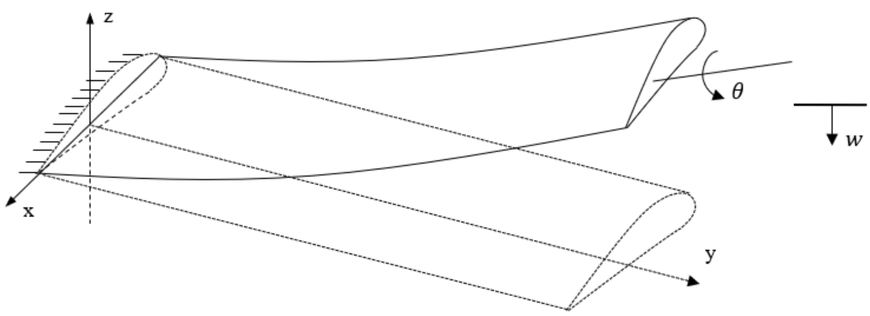

Figure 2.3 : Schematic representation of wing kinematics.

2.4 Free Vibration of Euler-Bernoulli Beam in Coupled Bending and Torsion

Prior to investigation the flutter behavior of an aircraft wing, the free vibration analysis is performed for bending-torsion coupling. The equations of motion of coupled bending-torsional vibration of Euler-Bernoulli beam are obtained by Hamilton's principle and then these equations are solved by DTM to achieve natural frequencies of the system.

The kinetic and potential energies of the aforementioned Euler-Bernoulli beam due to bending and torsion motion are expressed in equation 2.9-2.10, respectively.

$$T = \frac{1}{2}\int_0^l \left\{ \begin{bmatrix} \dot{w} \\ \dot{\theta} \end{bmatrix}^{\mathrm{T}} \begin{bmatrix} m & mX_\alpha \\ mX_\alpha & mR_\alpha^2 \end{bmatrix} \begin{bmatrix} \dot{w} \\ \dot{\theta} \end{bmatrix} \right\} dy \tag{2.9}$$

$$U = \frac{1}{2}\int_0^l \left\{ \begin{bmatrix} \partial^2 w/\partial y^2 \\ \partial\theta/\partial y \end{bmatrix}^{\mathrm{T}} \begin{bmatrix} EI & 0 \\ 0 & GJ \end{bmatrix} \begin{bmatrix} \partial^2 w/\partial y^2 \\ \partial\theta/\partial y \end{bmatrix} \right\} dy \tag{2.10}$$

The term m is the wing mass per unit length, X_α is the static unbalance and R_α is the radius of gyration. In order to obtain the governing differential equations, Hamilton's principle is followed in this section. Through the Hamilton's principle, integration by parts is implemented to eliminate the derivatives on the variations of the terms in equations. The standard variational statement for Hamilton's principle is defined as following,

$$\delta \int_{t_1}^{t_2} \mathcal{L} dt = 0 \tag{2.11}$$

where $\mathcal{L}$ is the Lagrangian of $T - U$. Rearranging equation 2.11,

$$\int_{t_1}^{t_1} \delta(T-U)\, dt = 0 \tag{2.12}$$

where t_1 and t_2 denotes the beginning and end of the time interval.

To obtain the governing differential equations of motion, variations of the kinetic and potential energy are taken as shown in the following expressions, respectively.

$$\delta T = \delta\left[\frac{1}{2}\int_0^l \left\{m\left(\frac{\partial w}{\partial t}\right)^2 + 2mX_\theta \frac{\partial w}{\partial t}\frac{\partial \theta}{\partial t} + mR_\theta^2\left(\frac{\partial \theta}{\partial t}\right)^2\right\} dy\right] \tag{2.13}$$

$$\delta U = \delta\left[\frac{1}{2}\int_0^l \left\{\frac{\partial^2}{\partial y^2}\left(EI\frac{\partial^2 w}{\partial y^2}\right) + \frac{\partial}{\partial y}\left(GJ\frac{\partial \theta}{\partial y}\right)\right\} dy\right] \tag{2.14}$$

Applying the integration by parts to equation 2.13-2.14, the variations of the kinetic energy and the potential energy have the final form as,

$$\delta T = \left\{m\frac{\partial w}{\partial t}\left(\delta\frac{\partial w}{\partial t}\right) + mX_\theta\left(\frac{\partial w}{\partial t}\delta\frac{\partial \theta}{\partial t} + \frac{\partial \theta}{\partial t}\delta\frac{\partial w}{\partial t}\right) + mR_\theta^2\frac{\partial \theta}{\partial t}\left(\delta\frac{\partial w}{\partial t}\right)\right\} dy \tag{2.15}$$

$$\begin{aligned}\delta U = \Bigg\{ & EI\frac{\partial^2 w}{\partial y^2}\left(\delta\frac{\partial w}{\partial y}\right)\Bigg|_0^l - \frac{\partial}{\partial y}\left(EI\frac{\partial^2 w}{\partial y^2}\right)\delta w\Bigg|_0^l + \int_0^l \frac{\partial^2}{\partial y^2}\left(EI\frac{\partial^2 w}{\partial y^2}\right)\delta w \\ & + GJ\frac{\partial \theta}{\partial y}\delta\theta\Bigg|_0^l - \int_0^l \frac{\partial}{\partial y}\left(GJ\frac{\partial \theta}{\partial y}\right)\delta\theta\Bigg\} dy\end{aligned} \tag{2.16}$$

By substituting equation 2.15-2.16 into equation 2.12, Hamilton's expression becomes,

$$\begin{aligned}\int_{t_1}^{t_2}\int_0^l \Bigg\{ & m\frac{\partial w}{\partial t}\left(\delta\frac{\partial w}{\partial t}\right) + mX_\theta\left(\frac{\partial w}{\partial t}\delta\frac{\partial \theta}{\partial t} + \frac{\partial \theta}{\partial t}\delta\frac{\partial w}{\partial t}\right) + mR_\theta^2\frac{\partial \theta}{\partial t}\left(\delta\frac{\partial \theta}{\partial t}\right) \\ & - \int_0^l \frac{\partial^2}{\partial y^2}\left(EI\frac{\partial^2 w}{\partial y^2}\right)\delta w - \int_0^l \frac{\partial}{\partial y}\left(GJ\frac{\partial \theta}{\partial y}\right)\delta\theta\Bigg\} dydt = 0\end{aligned} \tag{2.17}$$

Taking the coefficients of $\delta\omega$ and $\delta\theta$ respectively, the equations of motion are obtained as follows,

$$-\frac{\partial^2}{\partial y^2}\left(EI\frac{\partial^2 w}{\partial y^2}\right) + m\frac{\partial^2 w}{\partial t^2} + mX_\theta\frac{\partial^2 \theta}{\partial t^2} = 0 \tag{2.18}$$

$$\frac{\partial}{\partial y}\left(GJ\frac{\partial \theta}{\partial y}\right) + mR_\theta^2\frac{\partial^2 \theta}{\partial y^2} + mX_\theta\frac{\partial^2 w}{\partial t^2} = 0 \tag{2.19}$$

It is assumed that the motions in both bending and torsion are harmonic. Thus, the particular form that the solution to the boundary-value problem has these conditions obtain need be sought [49]. These conditions imply that $w(y,t)$ and $\theta(y,t)$ are of the exponential forms. The exponential function of time can be utilized as the general solution to the differential equations. The form of this solution is described in the following expressions,

$$
\begin{aligned}
w &= \overline{w}e^{i\omega t} \qquad\qquad & \dot{w} &= (i\omega)\overline{w}e^{i\omega t} \\
\theta &= \bar{\theta}e^{i\omega t} \qquad\qquad & \dot{\theta} &= (i\omega)\bar{\theta}e^{i\omega t}
\end{aligned}
\tag{2.20}
$$

where ω is the frequency of the motion, $\overline{w}$ and $\bar{\theta}$ are complex altitude functions of the span coordinate y. By the exponential solution function, the differential equations become independent of t and turn into ordinary differential equations with constant coefficients. The problem is considerably simplified by means of the exponential function. By implementing the exponential solution function to equation 2.18-2.19, the following expressions are obtained,

$$-\frac{\partial^2}{\partial y^2}\left(EI\frac{\partial^2\overline{w}}{\partial y^2}\right) + m\omega^2\overline{w} + m\omega^2X_\theta\bar{\theta} = 0 \tag{2.21}$$

$$\frac{\partial}{\partial y}\left(GJ\frac{\partial\bar{\theta}}{\partial y}\right) + mX_\theta\omega^2\overline{w} + mR_\theta^2\omega^2\bar{\theta} = 0 \tag{2.22}$$

Numerical evaluation can be significantly simplified by nondimensionalization. The definitions of the necessary dimensionless parameters for simplifying the expressions are given as follows,

$$\xi = \frac{y}{l} \qquad\qquad w = \frac{\overline{w}}{b} \qquad\qquad \bar{\theta} = \theta \tag{2.23}$$

Substituting these nondimensional parameters into equation 2.21-2.22, the governing equations in the nondimensional form are obtained,

$$-\frac{E_0I_0b}{l^4}\frac{\partial^2}{\partial\xi^2}\left(\sigma_{EI}\frac{\partial^2 w}{\partial\xi^2}\right) + mb\omega^2 w + m\omega^2X_\theta\theta = 0 \tag{2.24}$$

$$\frac{G_0J_0}{l^2}\frac{\partial}{\partial\xi}\left(\sigma_{GJ}\frac{\partial\theta}{\partial\xi}\right) + mbX_\theta\omega^2 w + mR_\theta^2\omega^2\theta = 0 \tag{2.25}$$

To simplify the equation 2.24-2.25, some necessary coefficients are introduced as following,

$$\lambda_1^4 = \frac{E_0 I_o}{m l^4} \qquad \lambda_2^4 = \frac{G_0 J_o}{m l^2} \tag{2.26}$$

These coefficients helps to rearrange the differential equations in simpler form. The finalized governing differential equations with the assumption of beam is homogenous, which implies that values of EI and GJ are constant, are given in equation 2.27-2.28.

$$-\lambda_1^4 \frac{1}{\omega^2} \frac{d^4 w}{d\xi^4} + w + \frac{X_\theta}{b}\theta = 0 \tag{2.27}$$

$$\lambda_2^2 \frac{1}{\omega^2} \frac{d^2 \theta}{d\xi^2} + \frac{X_\theta}{b} w + \frac{R_\theta^2}{b^2}\theta = 0 \tag{2.28}$$

2.5 Aeroelastic Flutter

In order to obtain the equations of motion for aeroelastic flutter, Hamilton's principle is utilized. The Hamilton's principle was introduced in Section 2.4. In addition to the statement of Hamilton's principle in Section 2.4, in this section, the virtual work is also added to this expression as given in equation 2.9.

$$\int_{t_1}^{t_1} \delta(T - U + W)\, dt = 0 \tag{2.29}$$

where t_1 and t_2 are the beginning and end of the time interval. The variation of the virtual work done on the system can be expressed as,

$$\delta W = -L\delta w + M\delta\theta \tag{2.30}$$

where L is the lift force and M is the aerodynamic moment which are given in equation 2.7-2.8 respectively.

The Hamilton's equation of Euler-Bernoulli beam without aerodynamic terms were expressed as following,

$$\begin{aligned} &\int_{t_1}^{t_2}\int_0^l \left\{ m\frac{\partial w}{\partial t}\left(\delta\frac{\partial w}{\partial t}\right) + mX_\theta\left(\frac{\partial w}{\partial t}\delta\frac{\partial \theta}{\partial t} + \frac{\partial \theta}{\partial t}\delta\frac{\partial w}{\partial t}\right) + mR_\theta^2\frac{\partial \theta}{\partial t}\left(\delta\frac{\partial \theta}{\partial t}\right) - \right. \\ &\left. \int_0^l \frac{\partial^2}{\partial y^2}\left(EI\frac{\partial^2 w}{\partial y^2}\right)\delta w - \int_0^l \frac{\partial}{\partial y}\left(GJ\frac{\partial \theta}{\partial y}\right)\delta\theta \right\} dydt = 0 \end{aligned} \tag{2.31}$$

The lift force and aerodynamic moment are placed into equation 2.31 according to the Hamilton's principle as follows,

$$\int_{t_1}^{t_2}\int_0^l\Big\{m\frac{\partial w}{\partial t}\left(\delta\frac{\partial w}{\partial t}\right)+mX_\theta\left(\frac{\partial w}{\partial t}\delta\frac{\partial\theta}{\partial t}+\frac{\partial\theta}{\partial t}\delta\frac{\partial w}{\partial t}\right)+mR_\theta^2\frac{\partial\theta}{\partial t}\left(\delta\frac{\partial\theta}{\partial t}\right)- \int_0^l\frac{\partial^2}{\partial y^2}\left(EI\frac{\partial^2 w}{\partial y^2}\right)\delta w-\int_0^l\frac{\partial}{\partial y}\left(GJ\frac{\partial\theta}{\partial y}\right)\delta\theta-L\delta w+M\delta\theta\Big\}dydt=0 \tag{2.32}$$

The equations of motion are expressed by taking the coefficients of $\delta\omega$ and $\delta\theta$ respectively as following,

$$-\frac{\partial^2}{\partial y^2}\left(EI\frac{\partial^2 w}{\partial y^2}\right)+m\frac{\partial^2 w}{\partial t^2}+mX_\theta\frac{\partial^2\theta}{\partial t^2}-L=0 \tag{2.33}$$

$$\frac{\partial}{\partial y}\left(GJ\frac{\partial\theta}{\partial y}\right)+\ mR_\theta^2\frac{\partial^2\theta}{\partial y^2}+mX_\theta\frac{\partial^2 w}{\partial t^2}+M\ =0 \tag{2.34}$$

The exponential function of time which is introduced in Section 2.4 is used as the general solution to the differential equations. By utilizing the exponential solution function, the equation 2.35-2.36 are rearranged as following,

$$-\frac{\partial^2}{\partial y^2}\left(EI\frac{\partial^2\overline{w}}{\partial y^2}\right)+m\omega^2\overline{w}+m\omega^2X_\theta\bar{\theta}-2\pi\rho_\infty U_\infty bC(k)\left[i\omega\overline{w}+U_\infty\bar{\theta}+b\left(\frac{1}{2}-a\right)i\omega\bar{\theta}\right]-\pi\rho_\infty b^2(-\omega^2\overline{w}+U_\infty i\omega\bar{\theta}+b\omega^2a\bar{\theta})=0 \tag{2.35}$$

$$\frac{\partial}{\partial y}\left(GJ\frac{\partial\bar{\theta}}{\partial y}\right)+mX_\theta\omega^2\overline{w}+mR_\theta^2\omega^2\bar{\theta}+b\left(\frac{1}{2}+a\right)\Big\{2\pi\rho_\infty U_\infty bC(k)\left[i\omega\overline{w}+U_\infty\bar{\theta}+b\left(\frac{1}{2}-a\right)i\omega\bar{\theta}\right]+\pi\rho_\infty b^2[-\omega^2\overline{w}+i\omega U_\infty\bar{\theta}+\omega^2ba\bar{\theta}]\Big\}-\pi\rho_\infty b^3\left[-\frac{1}{2}\omega^2\overline{w}+U_\infty i\omega\bar{\theta}-b\left(\frac{1}{8}-\frac{a}{2}\right)\omega^2\bar{\theta}\right]=0 \tag{2.36}$$

These complex equations can be simplified by nondimensionalization. The definitions of the necessary dimensionless parameters for simplifying the equations are as following,

$$\xi=\frac{y}{l} \qquad w=\frac{\overline{w}}{b} \qquad \bar{\theta}=\theta \tag{2.37}$$

These nondimensional parameters are substituted into the equation 2.35-2.36, dimensionless expressions are obtained as following,

$$-\frac{E_0I_0b}{l^4}\frac{d^2}{d\xi^2}\left(\sigma_{EI}\frac{d^2w}{d\xi^2}\right)+mb\omega^2w+m\omega^2X_\theta\theta-2\pi\rho_\infty U_\infty bC(k)\left[i\omega bw+U_\infty\theta+b\left(\frac{1}{2}-a\right)i\omega\theta\right]-\pi\rho_\infty b^2(-\omega^2bw+U_\infty i\omega\theta+b\omega^2a\theta)=0 \tag{2.38}$$

$$\frac{G_0 J_0}{l^2}\frac{d}{d\xi}\left(\sigma_{GJ}\frac{d\theta}{d\xi}\right) + mbX_\theta\omega^2 w + mR_\theta^2\omega^2\theta + b\left(\frac{1}{2} + a\right)\left\{2\pi\rho_\infty U_\infty bC(k)\left[i\omega bw + U_\infty\theta + \left(\frac{1}{2} - a\right)i\omega b^2\theta\right] + \pi\rho_\infty b^2[-b\omega^2 w + i\omega U_\infty\theta + \omega^2 ba\theta]\right\} - \pi\rho_\infty b^3\left[-\frac{1}{2}b\omega^2 w + U_\infty i\omega\theta - b\left(\frac{1}{8} - \frac{a}{2}\right)\omega^2\theta\right] = 0 \tag{2.39}$$

In addition to coefficients given in equation 2.26, new coefficient μ is introduced to simplify the equation 2.38-2.39 as following,

$$\mu = \frac{m}{\pi\rho_\infty b^2} \qquad \lambda_1^4 = \frac{E_0 I_o}{ml^4} \qquad \lambda_2^4 = \frac{G_0 J_o}{ml^2} \tag{2.40}$$

By using the parameters in equation 2.40, the simplified forms of equation 2.38-2.39 are obtained.

$$-\mu\lambda_1^4\frac{1}{\omega^2}\frac{d^4 w}{d\xi^4} + \mu w + \mu\frac{X_\theta}{b}\theta - l_w w - l_\theta = 0 \tag{2.41}$$

$$\mu\lambda_2^2\frac{1}{\omega^2}\frac{d^2\theta}{d\xi^2} + \mu\frac{X_\theta}{b}w + \mu\frac{R_\theta^2}{b^2}\theta + m_w w + m_\theta\theta = 0 \tag{2.42}$$

The complex dimensionless aerodynamic lift and moment coefficients l_w, l_θ, m_w and m_θ are listed as,

$$l_w = 2\frac{i}{k}C(k) - 1 \tag{2.43}$$

$$l_\theta = a + \frac{2}{k^2}C(k) + \frac{i}{k}\left[1 + 2\left(\frac{1}{2} - a\right)C(k)\right] \tag{2.44}$$

$$m_w = 2\frac{i}{k}C(k)\left(\frac{1}{2} + a\right) - a \tag{2.45}$$

$$m_\theta = 2\left(\frac{1}{2} + a\right)\frac{1}{k^2}C(k) - \frac{i}{k}\left(\frac{1}{2} - a\right)\left[1 - 2\left(\frac{1}{2} + a\right)C(k)\right] + a^2 + \frac{1}{8} \tag{2.46}$$

These aerodynamic coefficients generate oscillatory plunge and pitch motions by acting on a wing. The nondimensional aerodynamic coefficients l_w, l_θ, m_w and m_θ are functions of the reduced frequency, k. The widely-used parameter in aeroelasticity ,reduced frequency which is a measure of the unsteadiness of the flow, is expressed as following,

$$k = \frac{\omega b}{V} \tag{2.47}$$

The purpose of utilizing the aerodynamic lift and moment depending on the specific reduced frequency is that to facilitate the solution. The solution time of the numerical analysis is another difficulty that can be overcome by utilizing a reduced frequency. Thus, Theodorsen’s function significantly eases the solution by representing the changes in amplitude and phase of the unsteady aerodynamic forces and moments for variable frequency.

3. METHODOLOGY

This chapter is concerned with the methodology used for this thesis. Prior to implementing the differential transformation method (DTM) to the differential equations and associated boundary conditions, a brief technical overview of the utilized method in this study is given. Then, the k-method is introduced as a flutter solution method.

3.1 Differential Transformation Method

DTM is a powerful mathematical technique for solving ordinary and partial differential equations which can be applied to many engineering problems to obtain analytical solutions. This method basically based on Taylor series expansion. Taylor series method is less advantageous than DTM because it needs the symbolic computation of the necessary derivatives of the data functions [50]. The main distinction between the present technique and the Taylor series method is that the DTM has the capability of decreasing the size of computational work. By using DTM, following certain rules of transformation, the equations of motion are simplified to recurrence relations meanwhile the corresponding boundary conditions are transformed into a set of algebraic equations in terms of the differential transforms of the field variables [51]. As a solution of this algebraic iterating equations in the K domain, highly convergent and accurate results are obtained. The basic concept of the DTM are described as follows:

Let $f(x)$ be an analytical function in K domain and $x = x_0$ represent any point in K. Thus, the function $f(x)$ can be defined by a power series where the center is at x_0. $F(k)$ is referred to as the k^{th} order transformed function of original function $f(x)$ about the point $x = x_0$,

$$F(k) = \frac{1}{k!}\left[\frac{d^k f(x)}{dx^k}\right]_{x=x_0} \tag{3.1}$$

The inverse differential transform of the $f(x)$:

$$f(x) = \sum_{k=0}^{\infty} (x - x_0)^k F_k \tag{3.2}$$

Putting together equation 3.1-3.2:

$$f(x) = \sum_{k=0}^{\infty} \frac{(x - x_0)^k}{k!} \left[\frac{d^k f(x)}{dx^k}\right]_{x=x_0} \tag{3.3}$$

which is actually the expansion of the Taylor series for $f(x)$ about $x - x_0$.

Mathematical operations conducted by DTM are given in Table 3.1. Using these rules, governing equations are transformed into new expressions.

Table 3.1 : Main operations of the DTM.

Original Function	Transformed Function
$f(x) = u(x) \pm v(x)$	$F(k) = U(k) \pm V(k)$
$f(x) = au(x)$	$F(k) = aU(k)$
$f(x) = \frac{du(x)}{dx}$	$F(k) = (k+1)U(k+1)$
$f(x) = \frac{d^m u(x)}{dx^m}$	$F(k) = (k+1)(k+2) \ldots (k+m)U(k+m)$
$f(x) = u(x)v(x)$	$F(k) = \sum_{\iota=0}^{k} V(l)U(k-l)$

The boundary conditions of the system are also transformed by the DTM boundary condition rules which are given in Table 3.2.

Table 3.2 : Boundary Condition Relations of DTM.

$x=0$		$x=1$	
Original Boundary Conditions	Transformed Boundary Conditions	Original Boundary Conditions	Transformed Boundary Conditions
$f(0)=0$	$F(0)=0$	$f(1)=0$	$\sum_{k=0}^{\infty} F(k)=0$
$\frac{df}{dx}(0)=0$	$F(1)=0$	$\frac{df}{dx}(1)=0$	$\sum_{k=0}^{\infty} k.F(k)=0$
$\frac{d^2f}{dx^2}(0)=0$	$F(2)=0$	$\frac{d^2f}{dx^2}(1)=0$	$\sum_{k=0}^{\infty} k.(k-1).F(k)=0$
$\frac{d^3f}{dx^3}(0)=0$	$F(3)=0$	$\frac{d^3f}{dx^3}(1)=0$	$\sum_{k=0}^{\infty} k.(k-1).(k-2).F(k)=0$

3.2 Application of the Differential Transformation Method

By DTM rules, the governing equations for both investigation are transformed into new expressions. Referring to Table 3.1, the equations of motion and associated boundary conditions that are derived in Chapter 2 are transformed to new expressions, respectively.

3.2.1 Transformed equations for free vibrations of the coupled bending and torsion

The DTM is applied to the equations of motion for the free vibration of bending-torsional coupled beam. The transformed forms of equation 2.27-2.28 are given in equation 3.4-3.5, respectively.

$$\bar{w}[m+4]=\frac{\omega^2}{\lambda_1^4}\left(\frac{\bar{w}[m]+\bar{X}_\theta\bar{\theta}[m]}{(m+4)(m+3)(m+2)(m+1)}\right) \tag{3.4}$$

$$\bar{\theta}[m+2]=-\frac{\omega^2}{\lambda_2^2}\left(\frac{\bar{X}_\theta\bar{w}[m]+\bar{R}_\theta^2\bar{\theta}[m]}{(m+2)(m+1)}\right) \tag{3.5}$$

where $\bar{w}[m]$ and $\bar{\theta}[m]$ denote the transformed forms of the terms w and θ, respectively.

3.2.2 Transformed equations for aeroelastic flutter

By implementing the DTM rules to the aeroelastic equations of motion which are given in equation 2.41-2.42, the transformed equations of motion are given in the following expressions,

$$\bar{w}[m+4] = \frac{Z}{\lambda_1^4}\left(\frac{\bar{w}[m] + \bar{X}_\theta \bar{\theta}[m] - \frac{l_w}{\mu}\bar{w}[m] - \frac{l_\theta}{\mu}\bar{\theta}[m]}{(m+4)(m+3)(m+2)(m+1)}\right) \tag{3.6}$$

$$\bar{\theta}[m+2] = -\frac{Z}{\lambda_2^2}\left(\frac{X_\theta \bar{w}[m] + \bar{R}_\theta^2 \bar{\theta}[m] + \frac{m_w}{\mu}\bar{w}[m] + \frac{m_\theta}{\mu}\bar{\theta}[m]}{(m+2)(m+1)}\right) \tag{3.7}$$

Similarly, the DTM is applied to the associated boundary conditions. The transformed boundary conditions of the cantilevered Euler-Bernouilli beam are given in equation 3.8-3.11,

$$\bar{w}(0) = \bar{w}(1) = \bar{\theta}(0) = 0 \tag{3.8}$$

$$\sum_{k=0}^{\infty} k(k-1)\bar{w}(k) = 0 \tag{3.9}$$

$$\sum_{k=0}^{\infty} k(k-1)(k-2)\bar{w}(k) = 0 \tag{3.10}$$

$$\sum_{k=0}^{\infty} k\bar{\theta}(k) = 0 \tag{3.11}$$

3.3 The k-Method

The k-method, which is also known as American method, is based on the assumption of sinusoidal motion for the aeroelastic system. It is performed for the frequency domain solution. The k-method is generally very fast and quite simpler than other methods in determining the instability characteristics. The k-method is still popular in industry because of its speed. In this method, artificial damping parameter g is introduced to calculate the flutter speed of the system.

$$Z = \frac{(1+ig)}{\omega^2} \tag{3.12}$$

For the given specified reduced frequencies, the solution of the equation 3.6-3.7 gives Z. After Z is calculated, the frequency ω_i, the artificial damping g, and the flight speed V_i can be calculated from the following expressions,

$$\omega_i = \frac{1}{\sqrt{Re(Z)}} \tag{3.13}$$

$$g = \frac{Im(Z)}{Re(Z)} \tag{3.14}$$

$$V_i = \frac{\omega_i b}{k} \tag{3.15}$$

It is apparent from equation 3.15 that the value of k cannot be chosen as 0 in the k-method. The velocity versus damping $(V - g)$ and the velocity versus frequency $(V - f)$ diagrams are obtained by repeating the steps for varying range of k values. If there is no actual damping in the system where the artificial damping, g, first becomes positive, flutter is observed at this point. In the $(V - g)$ graph, the flutter instability can be observed at a point where the function g changes its sign from negative to positive.

4. FLUTTER ANALYSIS OF A SUBSONIC WING

This section presents the case studies and findings of this thesis. In the present study, a simple wing model is taken into consideration with pitch (bending) and plunge (torsion) motions. The solution of the aeroelastic system is obtained by k-method. The study designed to investigate the natural frequency, the flutter velocity and the flutter frequency. The case studies are performed in order to characterize the flutter phenomenon and also to obtain flutter values. The flutter instability is investigated for reference reduced frequencies. The obtained conventional $V - g$ plots enable determine a point where $g = 0$ on the flutter boundary.

4.1 Verification of the Numerical Method

To validate the accuracy and reliability of the developed algorithm, two wing types that are well known in literature are taken into consideration. Numerous studies related to aeroelastic analysis of Goland wing and HALE wing exist in literature. In order to determine the flutter values, the characteristic equation is solved for the reduced frequency value.

4.2 Validation Cases

As mentioned earlier, two wing models from open literature are analyzed for the dynamic characteristics. The numerical results obtained from DTM are presented both qualitatively and quantitatively. The results of these analyses are then compared with the findings from other studies in literature.

4.2.1 Goland wing

As a first step, the classical Goland wing is studied to demonstrate the capability of the current method. This case determines the natural frequency and flutter characteristics of cantilevered wing in coupled bending and torsion motion for the Goland wing. The Goland wing is a benchmark model that many researchers in aeronautical community have investigated for the purpose of comparisons and validations of structural and aeroelastic methods [52]. The Goland wing which is taken as a reference case for free vibration and flutter investigations, is a uniform and rectangular wing in a uniform flow. The wing has a well-defined natural frequencies, flutter velocity and flutter frequency.

4.2.1.1 Free vibration analysis of Goland wing for bending-torsion coupling

In this case, the free vibration analysis of Goland wing is performed to obtain natural frequencies. The structural and geometrical properties of Goland wing model used in validation process are given in Table 4.1.

Table 4.1 : The structural and geometrical properties of Goland wing model [33].

Parameter	Unit	Value
Half span (l)	m	6.096
Chord (c)	m	1.8288
Bending rigidity (EI)	$N.m^2$	9.77×10^6
Torsional rigidity (GJ)	$N.m^2$	0.987×10^6
Mass of the wing per unit length (m)	kg/m	35.71
Mass moment of inertia about elastic axis per unit length (I_{EA})	$kg.m$	8.64
Elastic axis position from leading edge (y_0)	m	$0.33c$
Static Unbalance	kg	6.523
Air density (ρ_∞)	kg/m^3	1.225

The coupled bending-torsional vibration chracteristics of Goland wing is investigated and compared with the study by Eslimy-Isfahany et al. [53]. The comparison of obtained first six natural frequencies of Goland wing are presented in Table 4.2.

Table 4.2 : First six natural frequencies of Goland wing.

Frequency (rad/s)			
Mode number	Present Study	Study of Ref. [53]	Error (%)
1	49.58	49.6	0.04
2	97.28	97.0	0.29
3	248.58	248.9	0.13
4	356.32	355.6	0.20
5	451.91	451.5	0.09
6	608.24	610.0	0.29

The results of current study listed in Table 4.2 are in line with the study by Eslimy-Isfahany et al. [53]. Moreover, the maximum error between findings is observed as 0.29%. The free vibration analysis of Goland wing for bending-torsion coupling is also performed by Hashemi and Richard et al. [54]. They found the first natural frequency as $49.62\ rad/s$, second natural frequency as $97.05\ rad/s$ and third natural frequency as $249\ rad/s$, which match with findings from DTM.

4.2.1.2 Flutter characteristics of Goland wing

Flutter analysis is also performed for Goland wing. By implementing the Goland wing parameters into the MATHEMATICA code, the flutter speed and the flutter frequency are obtained. The variation of the velocity with damping is shown in Figure 4.1.

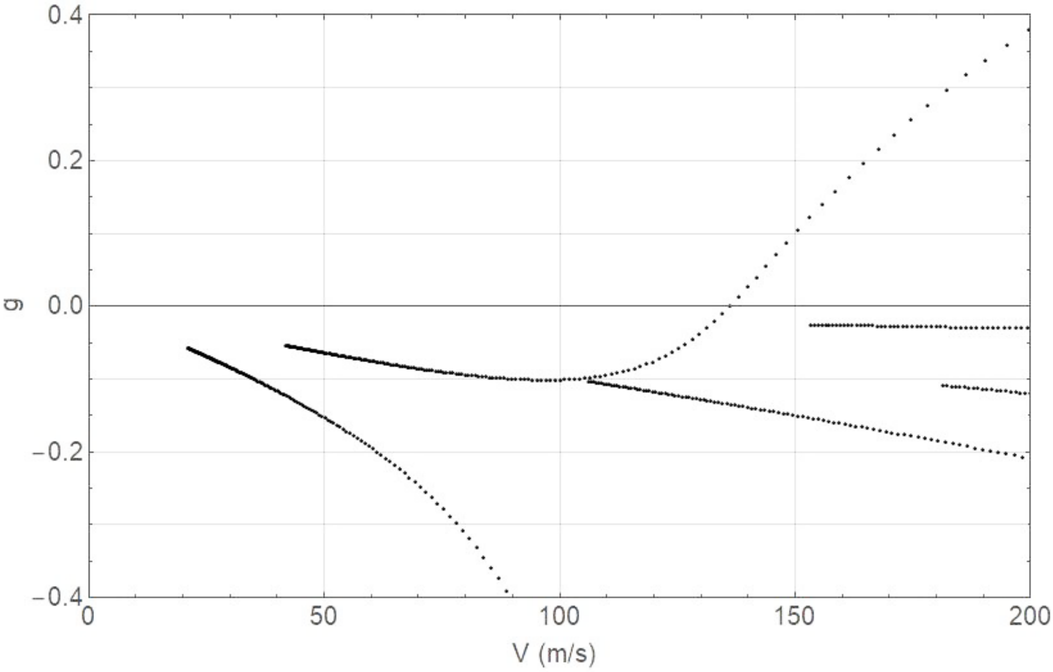

Figure 4.1 : Variation of velocity with damping for Goland wing.

$V - g$ plot is generally known as the classical flutter plot. It gives an estimate of the dynamic behaviour of the system easily. $V - g$ plot simply illustrates critical flow velocity where the function g changes its sign from negative to positive. Above the critical speed, the aerodynamic dampinf vanishes. The instability is occured at $V = 136.10\ m/s$. The variation of the frequency versus velocity and the variation of the frequency versus damping are illustrated in Figure 4.2 and Figure 4.3, respectively.

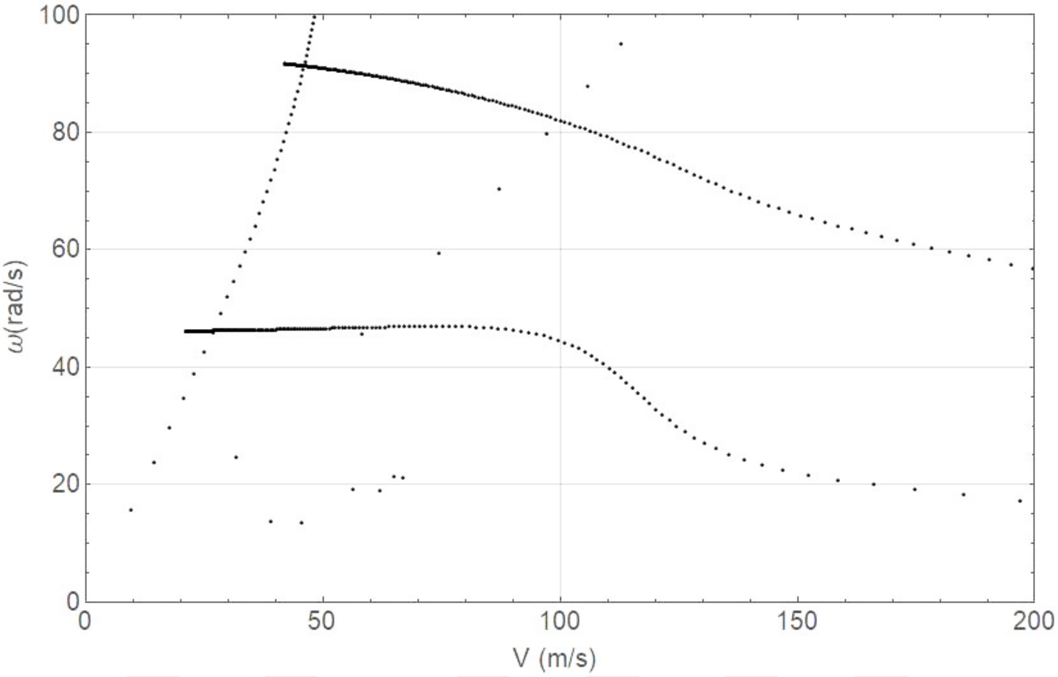

Figure 4.2 : Variation of velocity with frequency for Goland wing.

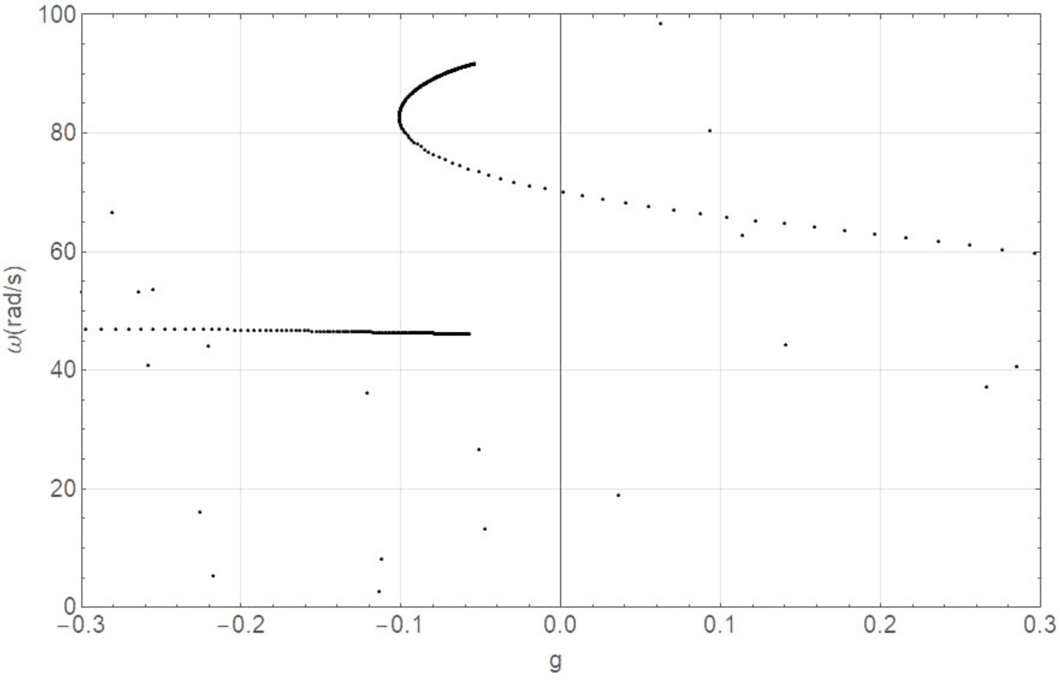

Figure 4.3 : Variation of frequency with damping for Goland wing.

The flutter frequency value can be determined where the value of damping is zero. It can be seen from Figure 4.3 that the value of the flutter frequency is observed as $\omega = 70.01\ rad/s$. Figure 4.3 indicates the excellent agreement between these results and those reported by Goland [24]. Patil and Hodges [33] also analyzed the flutter characteristics of Goland wing. The findings of current method are presented and compared with the reference study in Table 4.3.

Table 4.3 : The comparison of the flutter results for Goland wing model.

Critical values for flutter	Present Study	Reference Study [24]	Error (%)
Flutter Speed, m/s	136.10	137.16	0.77
Flutter Frequency, rad/s	70.01	70.70	0.97
Reduced Frequency	0.47	0.471	0.21

It can be seen from Table 4.3 that the flutter results obtained from DTM are in good agreement with the reference study. A possible explanation for these results may be related to the accuracy of the developed algorithm. Similar investigations are also performed by Matter [1] and Patil [33]. Matter et al. [1] investigated the flutter characteristics of Goland wing by Galerkin method. They found the flutter speed as 136.41 m/s and flutter frequency as 69.35 rad/s. Patil and Hodges [33] also analyzes the flutter boundaries of Goland wing. They reported the flutter speed as 137.16 m/s and flutter frequency as 70.2 rad/s which are very close to findings of the current study.

4.2.2 HALE wing

HALE aircraft is equipped with light wings of high aspect ratio, as shown in Figure 4.4, which increase the aerodynamic efficiency by maximizing lift-to drag ratio and endurance. Besides its advantages, it may undergo large deformations due to presence of geometric nonlinearities while operating in conditions including slow maneuvers at high altitudes and low speeds. The geometrical nonlinearities due to large amplitude deflection may reduce the flutter speed and frequency and induce more complex dynamic behavior.

Figure 4.4 : Schematic view of HALE aircraft [55].

These aircraft are susceptible to dynamic instabilities, such as flutter and large-amplitude limit cycle oscillations (LCOs). The types of nonlinearities can be defined as inertial (due to the location of concentrated or distributed masses), aerodynamic (due to dynamic stall, large oscillations leading to flow separation, and oscillating shocks), and structural (due to large deflections/rotations, material behavior, and dissipation) [56].

4.2.2.1 Free vibration analysis of HALE wing for bending-torsion coupling

In this case, the free vibration analysis of HALE wing in coupled bending and torsion motions is performed. The structural and geometrical properties of HALE wing model used in validation process are given in Table 4.4.

Table 4.4 : The structural and geometrical properties of the HALE wing model.

Parameter	Unit	Value
Half span (l)	m	16
Chord (c)	m	1
Bending rigidity (EI)	$N.m^2$	2×10^{14}
Torsional rigidity (GJ)	$N.m^2$	1×10^{14}
Mass of the wing per unit length (m)	kg/m	0.75
Mass moment of inertia about elastic axis per unit length (I_{EA})	$kg.m$	0.1
Elastic axis position from leading edge (y_0)	m	$0.5c$
Static Unbalance	kg	0
Altitude	km	20
Air density (ρ_∞)	kg/m^3	0.0889

The coupled bending-torsional free vibration of HALE wing is analyzed to achieve the natural frequencies. The first four natural frequencies of HALE wing for bending-torsion coupling are presented and compared with reference study in Table 4.5.

Table 4.5 : First four natural frequencies of HALE wing.

	Frequency (rad/s)		
Mode number	Present Study	Reference Study [31]	Error (%)
1	2.24	2.24	0%
2	14.06	14.06	0%
3	31.05	31.07	0.06%
4	39.36	39.36	0%

The first four natural frequencies obtained from current study are compared with the study by Patil et al. [31] in Table 4.5. It can be deduced that the findings are in excellent agreement. The natural frequencies are exactly the same except the third mode, which has already very low error percentage.

4.2.2.2 Flutter characteristics of HALE wing

This case analyzes the flutter boundaries of HALE wing. Flutter speed and frequency values are obtained by observing the relevant plots of the system. By developed algorithm, the graphs of flutter analysis with respect to velocity, frequency and damping are obtained. The velocity and damping relation for each mode is illustrated in Figure 4.5.

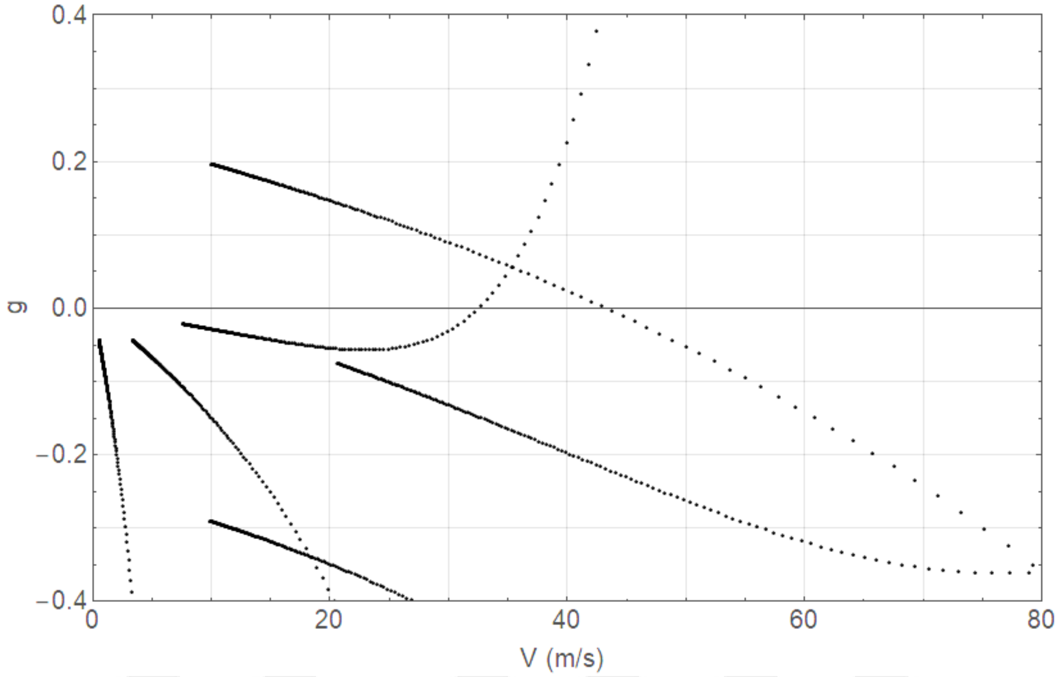

Figure 4.5 : Variation of velocity with damping for HALE wing.

In a linear system, flutter is the point at which zero-damping is displayed. The flutter velocity versus damping graph is obtained via the k-method which were introduced in detail in Section 3.3. The sign of damping value changes from negative to positive which is an indicator of the occurrence of the flutter. It can be seen that the instability exists where $g = 0$, which also corresponds to aircraft velocity of $32.22\ m/s$.

Figure 4.6 and Figure 4.7 present the variation of velocity with frequency and the variation of the frequency with damping for each mode, respectively.

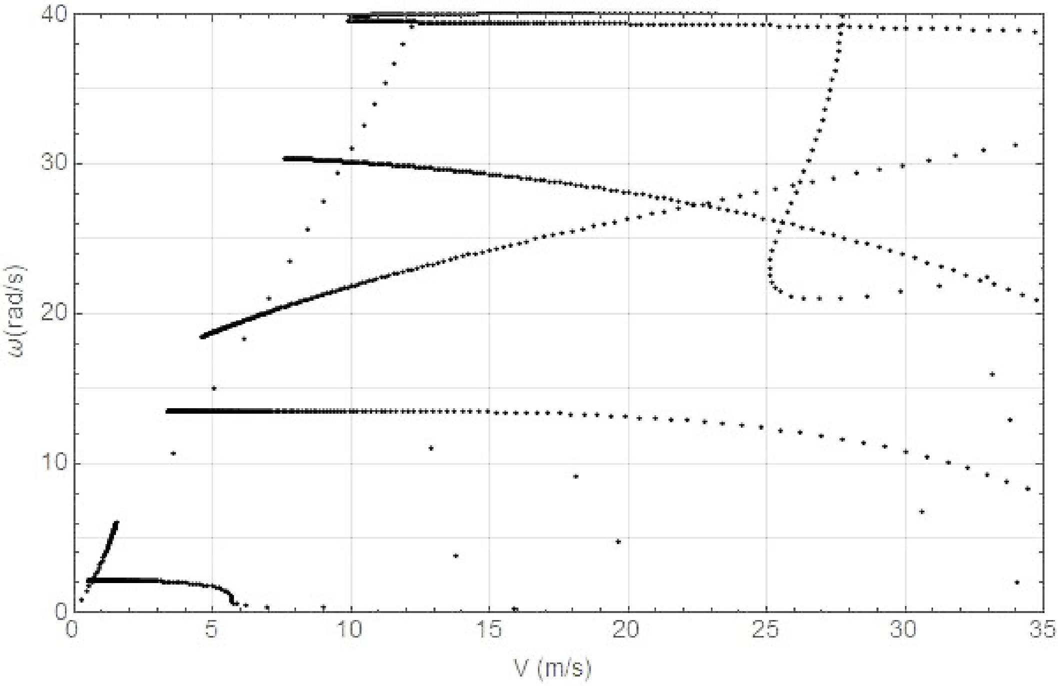

Figure 4.6 : Variation of velocity with frequency for HALE wing.

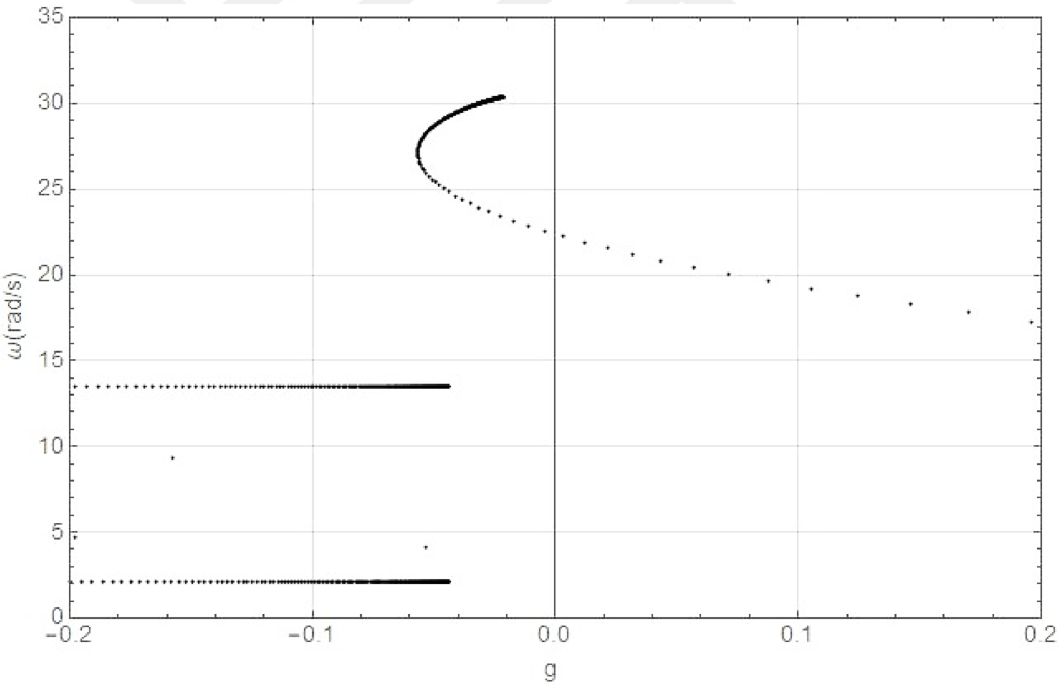

Figure 4.7 : Variation of frequency with damping for HALE wing.

The flutter velocity was found as 32.22 m/s. The frequency corresponding to this velocity for the HALE wing is found as 22.39 rad/s and is the flutter frequency. There has been several methods to investigate the flutter characteristics. The findings of the current study match those observed in earlier studies. Patil et al. [31] also analyzed the flutter frequency of HALE wing. They found the flutter frequency as

22.61 rad/s, which indicates the excellent agreement with the findings from the current study. Table 4.6 below presents the comparison of main flutter characteristics of the HALE wing.

Table 4.6 : The comparison of flutter results for the HALE wing model.

Critical values for flutter	Present study	Analytical study [31]	Error (%)
Flutter Speed, m/s	32.22	32.21	0.03
Flutter Frequency, rad/s	22.39	22.61	0.97
Reduced Frequency	0.347	0.350	0.86

Table 4.6 provides the flutter data for the aircraft model which is under investigation. Closer inspection of the Table 4.6 shows that the flutter data obtained by DTM are matched up with the studies from literature. The critical behavior of HALE wing is studied to validate the algorithm. These results corroborate with the findings of the study in literature [31]. It is encouraging to compare this results also with those found by Patil et al. [31] who found flutter speed as 32.21 m/s. The similar investigation of the HALE wing is conducted by Arena et al. [56]. They analyzed the flutter behavior of HALE wing and reported the critical velocity as 31 m/s.

5. VARIABLE-SPAN MORPHING WINGS

Span morphing concept has ability to changing the wing span substantially to achieve better aircraft performance, enlarge the flight envelope and accomplish multiple mission roles at different phases of flight. This technology increases the flight efficiency at high and low speeds since the wing span is one of the most important parameters for air vehicles. Wings with large span have good range and fuel efficiency. Thus, as span increases, longer flight range and more fuel savings are obtained easily. Furthermore, span morphing mechanism enables to achieve high-speed flight, better aircraft maneuverability and relatively higher cruise speed by shortening of wing span. Moreover, asymmetrical wing span extension is capable of provide roll control as an alternative to aileron control surfaces [57].

Span morphing concepts can be categorized in two main sections: in-plane shape changing-primarily through telescopic span mechanism or out-of-plane movement with items such as folding tips [58].

Not only the aerodynamic effects should be taken into consideration, but also the structural complexity should be accounted for. Unfortunately, the wing root bending moment increases as span increases and causes to increase in wing structural mass. Thus, loading on wing is more severe which causes to higher deformation. The stiffness and aerodynamic shape also change quickly due to span morphing so that aeroelastic characteristics such as flutter speed, dynamic response, and static load changes [58]. The flexibility of the wing is affected by the aspect ratio and reverse aeroelastic effects can be seemed. Several investigations were performed to explore aeroelastic characteristics of morphing aircraft up to now. The studies about the effects of span wing morphing to aeroelastic behavior of an aircraft shows that the span wing extension reduces the flutter speed. Thus, the aerodynamic, structural, aeroelastic and control characteristics of span morphing aircraft should be analyzed carefully.

5.1 Validation Cases for Variable-Span Morphing Wings

Prior to analyzing the flutter characteristics of morphing wings, numerous validation cases are conducted to ensure that the stepped beam model works well. The wing is modeled as a stepped Euler-Bernoulli beam by dividing it into three equal segments as shown in Figure 5.1.

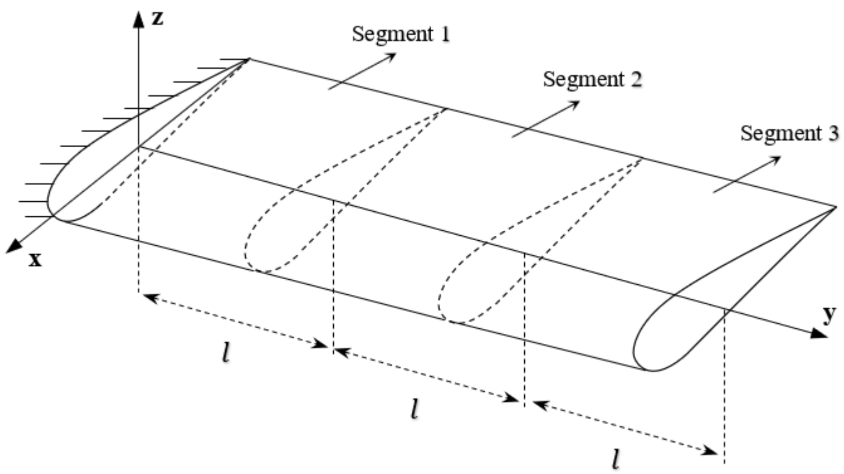

Figure 5.1 : Schematic view of the variable-span morphing wing model with three equal segments.

The boundary conditions of Euler-Bernoulli beam for one-segment model were introduced in Chapter 2. The boundary conditions of three-stepped beam for bending and torsion motions are given in Table 5.1Table 5.1 as following,

Table 5.1 : Bending and torsion boundary conditions of three-stepped beam model.

Fixed end		Free end	
Bending	Torsion	Bending	Torsion
$w_1(t, y_1 = 0) = 0$	$\theta_1(t, y_1 = 0) = 0$	$\dfrac{\partial^2 w_3(t, y_3 = l_3)}{\partial {y_3}^2} = 0$	$\dfrac{\partial \theta_3(t, y_3 = l_3)}{\partial y_3} = 0$
$\dfrac{\partial w_1(t, y_1 = 0)}{\partial y_1} = 0$		$\dfrac{\partial^3 w_3(t, y_3 = l_3)}{\partial {y_3}^3} = 0$	

The half span of wing is the only parameter that changes. All other parameters remain the same since they are related with cross-section of the wing. The relations of the structural and geometrical properties of each segment for the multi-segment wing model are given in Table 5.2 as following,

Table 5.2 : Structural and geometrical properties for each segment of three-stepped wing model.

Parameter	Unit	Segment 1	Segment 2	Segment 3
Half span (l)	m	l_1	l_2	l_3
Chord (c)	m	c_1	c_2	c_3
Bending rigidity (EI)	$N.m^2$	EI_1	EI_2	EI_3
Torsional rigidity (GJ)	$N.m^2$	GJ_1	GJ_2	GJ_3
Mass of the wing per unit length (m)	kg/m	m_1	m_2	m_3
Mass moment of inertia about elastic axis per unit length (I_{EA})	$kg.m$	$I_{\theta 1}$	$I_{\theta 2}$	$I_{\theta 3}$
Elastic axis position from leading edge (y_0)	m	a_1	a_2	a_3
Static Unbalance	kg	$S_{\alpha 1}$	$S_{\alpha 2}$	$S_{\alpha 3}$

The bending and torsion continuity conditions for the first and second step of three-stepped beam model are given in Table 5.3 and Table 5.4, respectively.

Table 5.3 : Bending and torsion continuity conditions in the first step of three-stepped beam.

Bending	Torsion
$w_1(t, y_1 = l_1) = w_2(t, y_2 = 0)$	$\theta_1(t, y_1 = l_1) = \theta_2(t, y_2 = 0)$
$\dfrac{\partial w_1(t, y_1 = l_1)}{\partial y_1} = \dfrac{\partial w_2(t, y_2 = 0)}{\partial y_2}$	$\dfrac{\partial \theta_1(t, y_1 = l_1)}{\partial y_1} = \dfrac{(GJ)_2}{(GJ)_1}\dfrac{\partial \theta_2(t, y_2 = 0)}{\partial y_2}$
$\dfrac{\partial^2 w_1(t, y_1 = l_1)}{\partial {y_1}^2} = \dfrac{(EI)_2}{(EI)_1}\dfrac{\partial^2 w_2(t, y_2 = 0)}{\partial {y_2}^2}$	
$\dfrac{\partial^3 w_1(t, y_1 = l_1)}{\partial {y_1}^3} = \dfrac{(EI)_2}{(EI)_1}\dfrac{\partial^3 w_2(t, y_2 = 0)}{\partial {y_2}^3}$	

Table 5.4 : Bending and torsion continuity conditions in the second step of three-stepped beam.

Bending	Torsion
$w_2(t, y_2 = l_2) = w_3(t, y_2 = 0)$	$\theta_2(t, y_2 = l_2) = \theta_3(t, y_3 = 0)$
$\dfrac{\partial w_2(t, y_2 = l_2)}{\partial y_2} = \dfrac{\partial w_3(t, y_3 = 0)}{\partial y_3}$	$\dfrac{\partial \theta_2(t, y_2 = l_2)}{\partial y_2} = \dfrac{(GJ)_3}{(GJ)_2}\dfrac{\partial \theta_3(t, y_3 = 0)}{\partial y_3}$
$\dfrac{\partial^2 w_2(t, y_2 = l_2)}{\partial {y_2}^2} = \dfrac{(EI)_3}{(EI)_2}\dfrac{\partial^2 w_3(t, y_3 = 0)}{\partial {y_3}^2}$	
$\dfrac{\partial^3 w_2(t, y_2 = l_2)}{\partial {y_2}^3} = \dfrac{(EI)_3}{(EI)_2}\dfrac{\partial^3 w_3(t, y_3 = 0)}{\partial {y_3}^3}$	

5.1.1 Natural frequencies of three-stepped Goland wing

This case investigates the natural frequencies of three-stepped Goland wing. For three-segment Goland wing analysis, it is aimed to achieve the same natural frequency values with those of the original one-segment Goland wing. Table 5.5 compares the first six natural frequencies of three-segment Goland wing with findings from one-segment Goland wing.

Table 5.5 : The comparison of the natural frequencies of three-segment and one-segment Goland wing models.

Frequency (rad/s)			
Mode number	Three-segment	One-segment	Error (%)
1	49.58	49.58	0
2	97.28	97.28	0
3	248.58	248.59	0.004
4	356.32	356.33	0.003
5	451.91	451.90	0.002
6	608.24	610.00	0.29

As can be seen from the Table 5.5**Error! Reference source not found.**, first two modes have exactly the same value whilst other modes are almost the same. These findings demonstrate that the three-stepped model works well.

5.1.2 Flutter characteristics of three-stepped Goland wing

To validate the flutter characteristics of three-segment Goland wing, the original Goland wing is modelled as three-stepped Euler-Bernoulli beam. All of the parameters except the half span length for each segment are taken exactly the same with the original Goland wing parameters. The half span length of each segment is one-third of the half span length of original Goland wing. The variation of flutter speed with damping for three stepped Goland wing model is given in Figure 5.2.

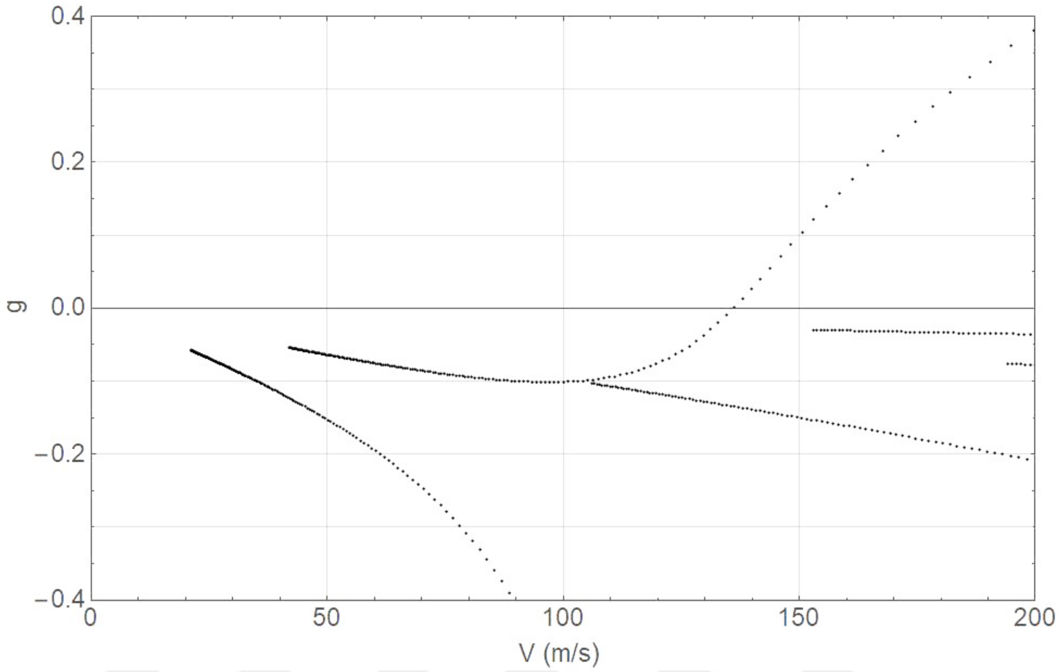

Figure 5.2 : Variation of speed with damping for three-stepped Goland wing model.

As can be seen from the Figure 5.2, flutter instability can be sight at where the g changes its sign from negative to positive. The flutter speed and flutter frequency are found as 136.10 m/s and 70.01 rad/s respectively. It can be deduced from these findings that three-segment Goland wing has same flutter values with one segment Goland wing.

The variation of speed with frequency and the variation of frequency with damping for three-segment Goland wing are given in Figure 5.3 and Figure 5.4, respectively.

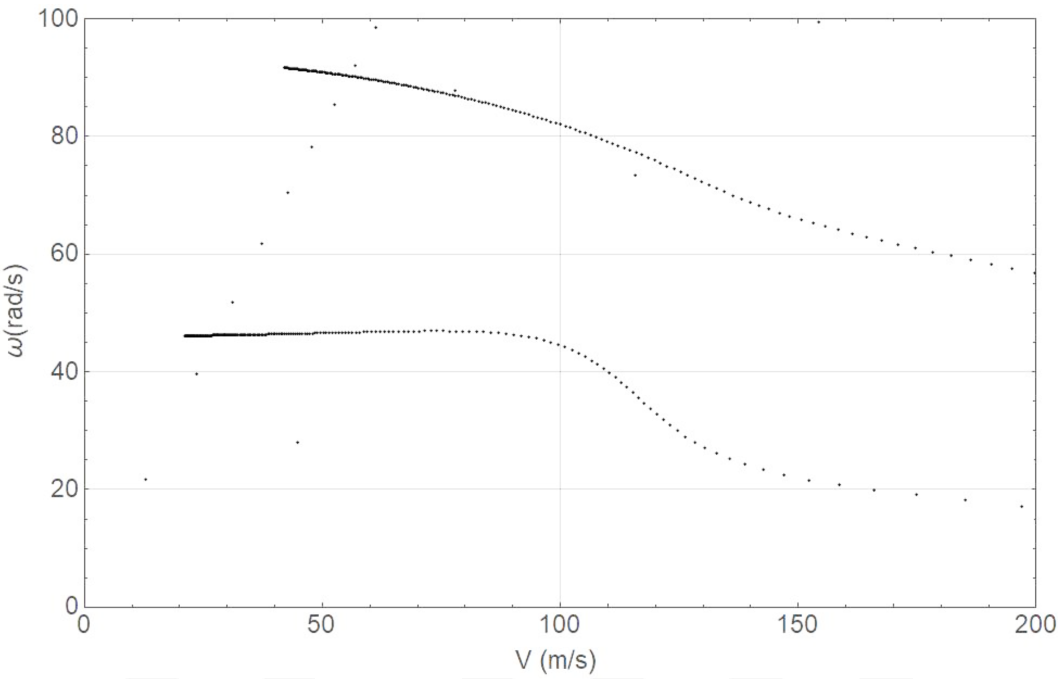

Figure 5.3 : Variation of speed with frequency for three-stepped Goland wing.

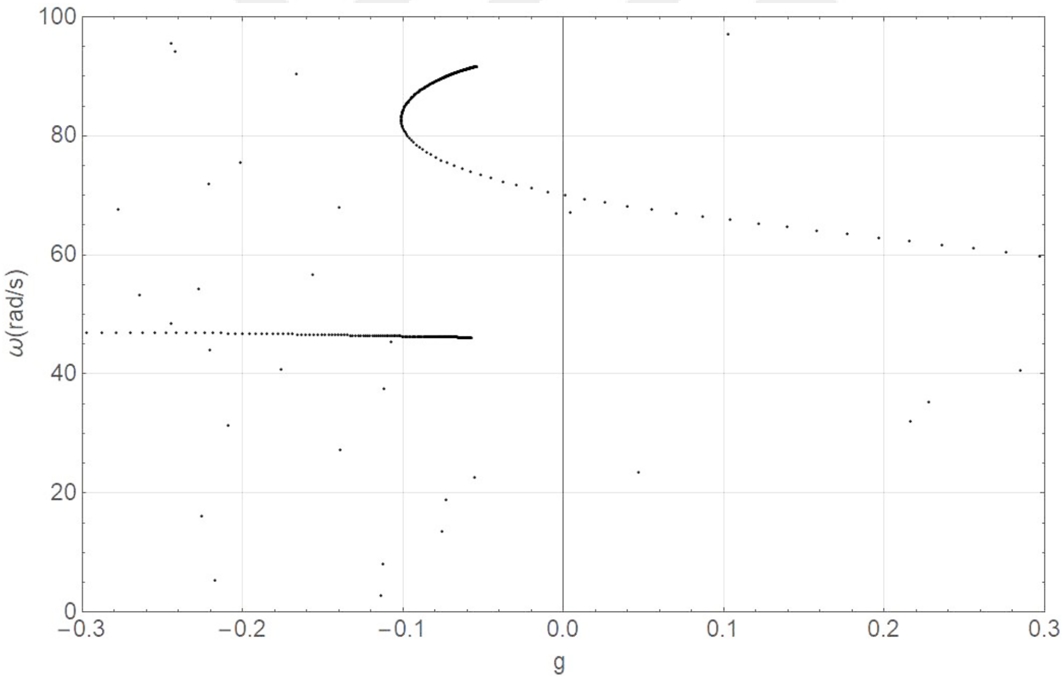

Figure 5.4 : Variation of frequency with damping for three-stepped Goland wing.

The flutter frequency is observed at a point where the damping is zero. The flutter frequency of three equal segment wing is found as $70.01\ rad/s$ which is in good agreement with the flutter frequency of one segment Goland wing [24].

Table 5.6 compares the flutter characteristics of one-segment and three-segment Goland wing models. The findings of one-segment model were found in Chapter 4.

Table 5.6 : The comparison of the flutter values of three-segment and one-segment Goland wing models.

Critical values for flutter	Three-segment	One-segment	Error (%)
Flutter Speed, m/s	136.10	136.10	0
Flutter Frequency, rad/s	70.01	70.01	0
Reduced Frequency	0.47	0.47	0

Table 5.6 shows that the flutter speed and flutter frequency exactly the same for both two configurations.

5.1.3 Natural frequencies of three-stepped HALE wing

In this case, HALE wing is modelled as a three-stepped beam to represent the morphing wing concept. The semi-span length of HALE wing is divided into three equal lengths. Other parameters of each segment are equal to the HALE wing parameters. By this configuration, it is aimed to obtained the same natural frequencies with one-segment HALE wing. The first six natural frequencies for each configuration are given in Table 5.7.

Table 5.7 : The comparison of the natural frequencies of three-segment and one-segment HALE wing models.

	Frequency (rad/s)		
Mode number	Three-segment	One-segment	Error (%)
1	2.24	2.24	0
2	14.06	14.06	0
3	31.05	31.05	0
4	39.36	39.36	0
5	77.12	77.12	0
6	93.14	93.14	0

From the Table 5.7 we can see that both configurations have same natural frequency values as it should be.

5.1.4 Flutter characteristics of three-stepped HALE wing

The flutter analysis of three-segment wing is also repeated by using HALE wing. The semi-span length of HALE wing is divided into three equal parts. As in the previous cases, the parameters of each segment are taken equal to HALE wing parameters. The variation of flutter speed with damping for three-segment HALE wing model is illustrated in Figure 5.5.

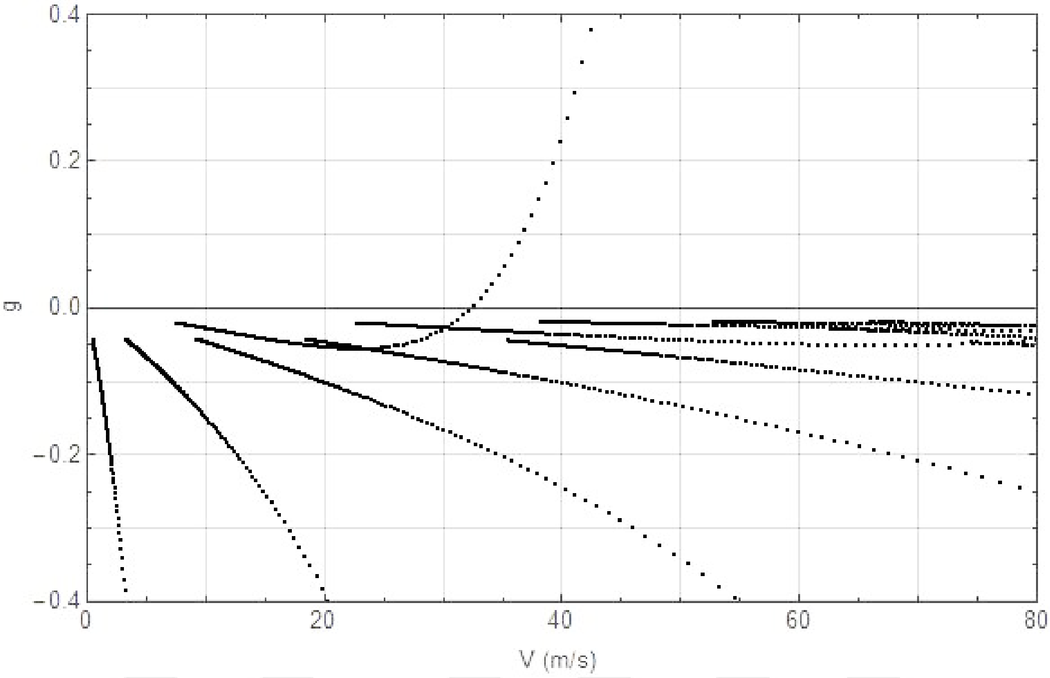

Figure 5.5 : Variation of speed with damping for three-segment HALE wing.

By analyzing the three-stepped HALE wing model, the flutter speed is found as $32.22\ m/s$ which is exactly the same with one-segment original HALE wing. The variation of speed with frequency and variation of frequency with damping for three-segment HALE wing are given in Figure 5.6 and Figure 5.7, respectively.

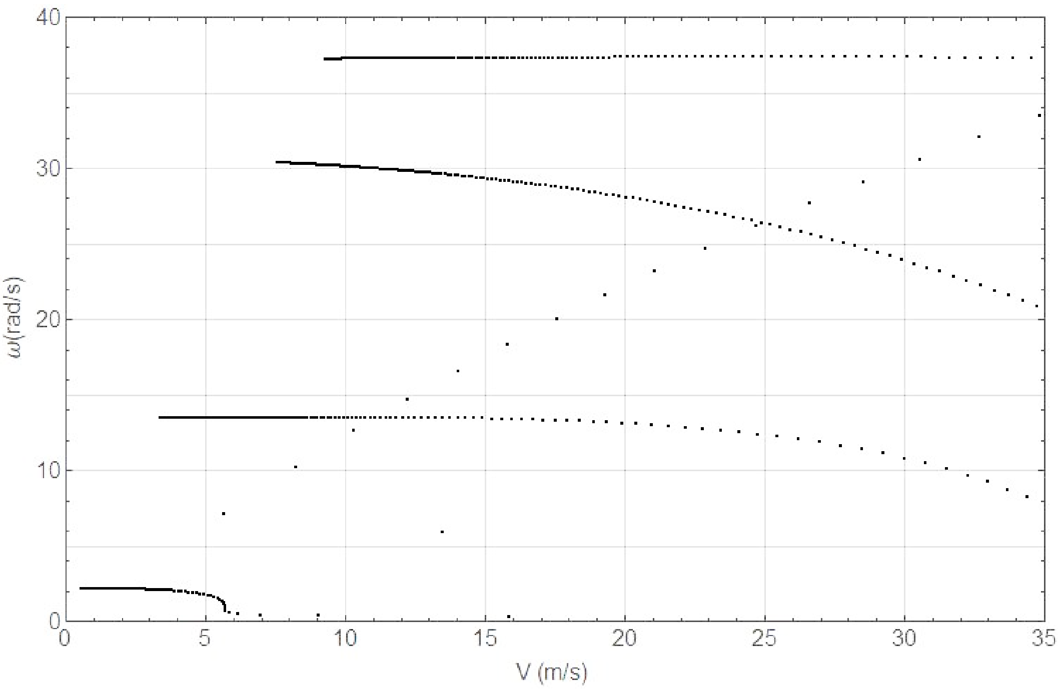

Figure 5.6 : Variation of speed with frequency for three-segment HALE wing.

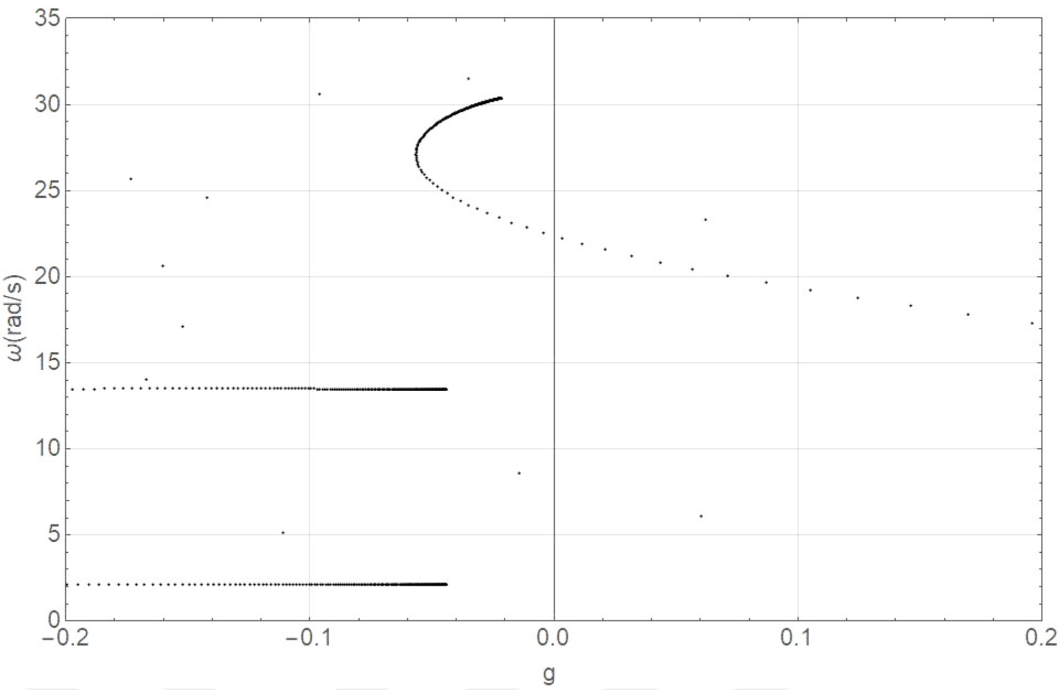

Figure 5.7 : Variation of frequency with damping for three-segment HALE wing.

As can be seen from Figure 5.7, the flutter frequency is found again as $22.39 \ \mathrm{rad/s}$. The same value was found in Chapter 4.2.2 by analyzing the one-segment HALE wing model. The flutter speed and flutter frequency of three-segment HALE wing are compared with the flutter values of one-segment HALE wing which were found in Chapter 4. The findings are presented in Table 5.8.

Table 5.8 : The comparison of the flutter values of three-segment and one-segment HALE wing models.

Critical values for flutter	Three-segment	One-segment	Error (%)
Flutter Speed, m/s	32.22	32.22	0
Flutter Frequency, rad/s	22.39	22.39	0
Reduced Frequency	0.347	0.347	0

It can be seen from the data in Table 5.8 that the flutter values obtained from both configurations are exactly the same, which is an expected outcome. Thus, the verification study for three-segment HALE wing model is successfully completed.

5.1.5 Natural frequencies of Goland wing with three different segments

Another case study is conducted on the purpose of validating the three-segment wing model of Hashemi and Richard [59]. They investigate the free vibration of three-segment wing model which is composed of parts with different properties. The Goland wing is also used as the basis for this case but some parameters are changed in the study of Hashemi and Richard [59]. The structural and geometrical parameters of the wing model used in validation study are listed in Table 5.9. In this case, lengths of each segment are equal and taken as 2 m.

Table 5.9 : The structural and geometrical parameters of the wing model used in reference study.

Parameter	Unit	Value
Half span (l)	m	6
Bending rigidity (EI)	$N.m^2$	9.75×10^6
Torsional rigidity (GJ)	$N.m^2$	0.988×10^6
Mass of the wing per unit length (m)	kg/m	35.75
Mass moment of inertia about elastic axis per unit length (I_{EA})	kg/m	8.64
Elastic axis position from leading edge (y_0)	m	$0.33c$
Static Unbalance	kg	6.523
Air density (ρ_∞)	kg/m^3	1.225

The schematic view of three-segment wing model is illustrated in Figure 5.8. As indicated in the study [59], Goland wing properties are used for the first segment of wing. The properties of second segment are taken as two-third of segment 1 and the properties of third segment are taken as one-third of segment 1.

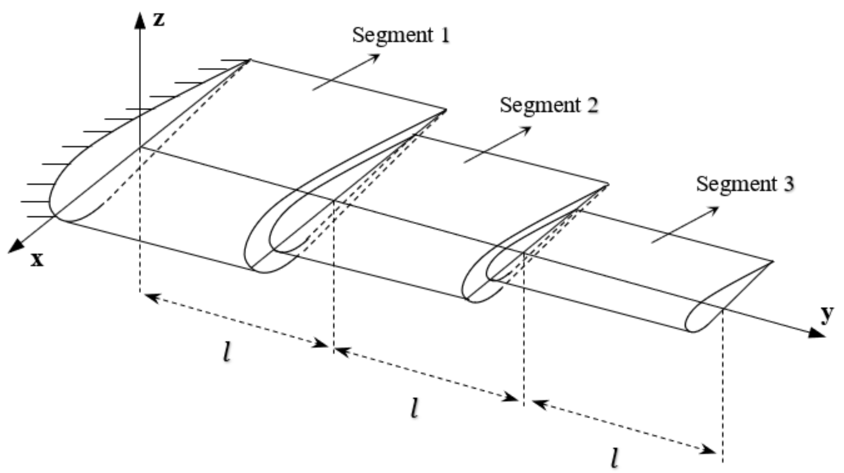

Figure 5.8 : Schematic view of the variable-span morphing wing model with three different segments.

The findings of current study are given and compared with findings from literature in Table 5.10. It can be seen from Table 5.10 that the results are very close to the study of Hashemi and Richard [59].

Table 5.10 : The comparison of the natural frequencies of three-stepped Goland wing.

Frequency (rad/s)			
Mode number	Present Study	Reference Study [59]	Error (%)
1	74.02	74.43	0.55
2	131.20	128.57	2
3	248.42	253.40	1.96
4	386.16	376.59	2.48
5	425.19	431.29	1.41

The chord length information is not stated in the study of Hashemi and Richard [59]. Therefore, the chord lengths of each segment is taken as the same with Goland wing in this study. Thus, it is estimated by the author that the errors may result from the missing reference data.

5.1.6 Flutter characteristics of Goland wing with three different segments

After validating the natural frequencies of three-stepped Goland wing with different segments, the flutter behavior is also analyzed in this case. The variation of speed with damping for three-stepped Goland wing with different segments is illustrated in Figure 5.9.

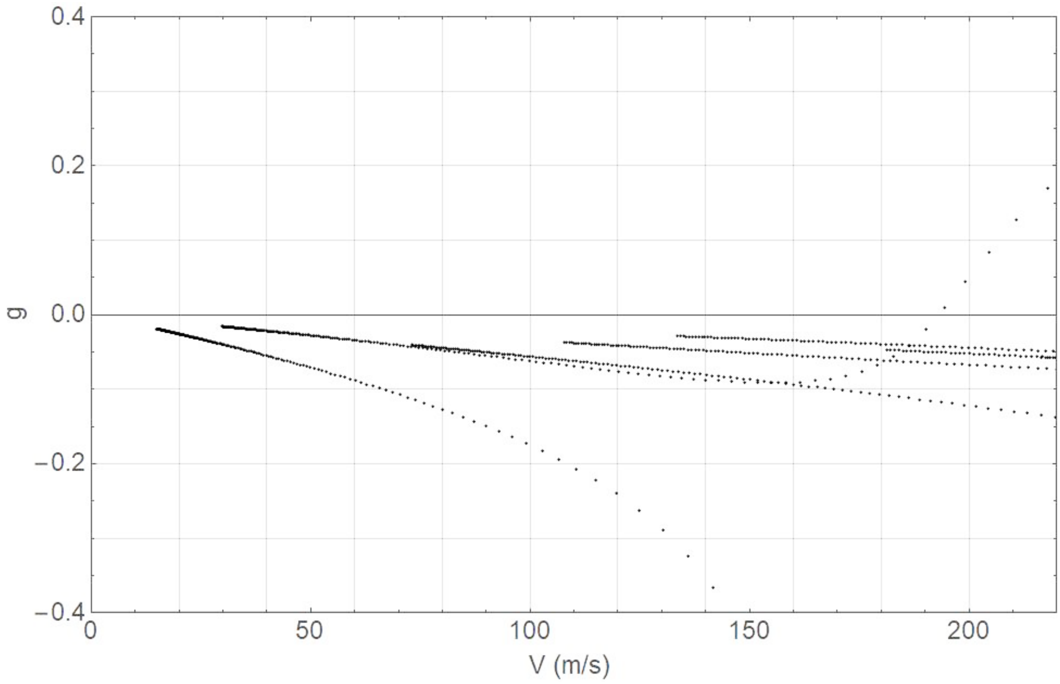

Figure 5.9 : Variation of speed with damping for three-stepped Goland wing with different segments.

The instability point can also be seen from Figure 5.9. The flutter speed is found as $\mathbf{193.1}\ \boldsymbol{m/s}$ where the damping changes its sign from negative to positive. The variation of frequency with damping for three-stepped Goland wing with different segments is given in Figure 5.10.

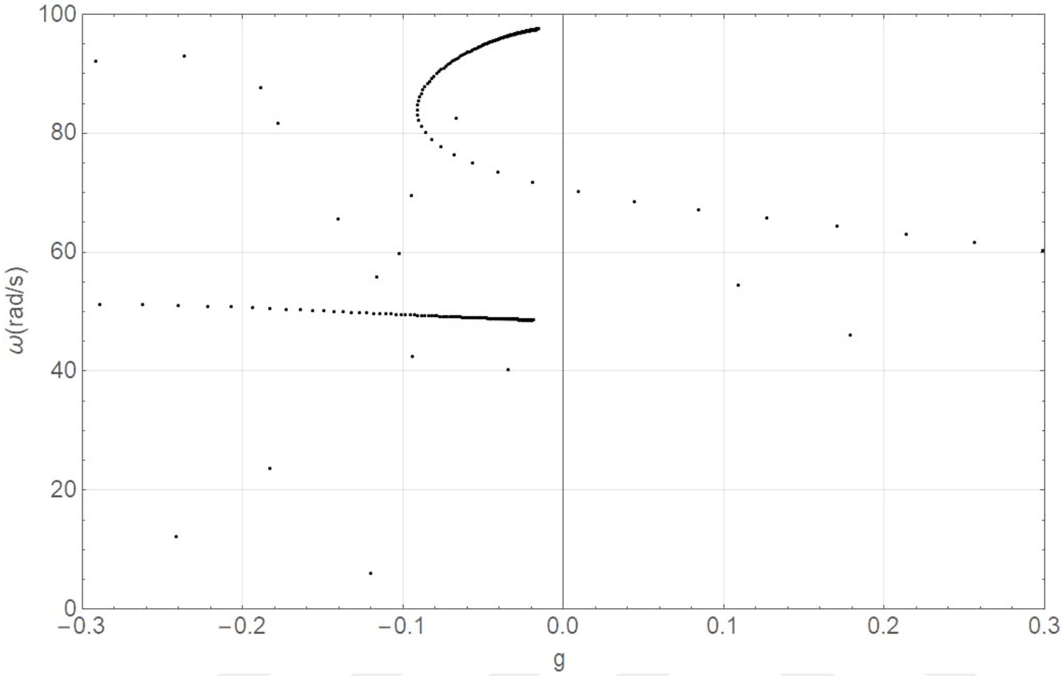

Figure 5.10 : Variation of frequency with damping for three-stepped Goland wing with different segments.

The critical frequency value for three-stepped Goland wing with different segments is found from Figure 5.10 as $70.5\ rad/s$. The flutter speed and flutter frequency values are presented in Table 5.11.

Table 5.11 : Flutter characteristics of three-stepped Goland wing with different segments.

Critical values for flutter	Current Study
Flutter Speed, m/s	193.1
Flutter Frequency, rad/s	70.5

Flutter frequency of Goland wing was found as $136.10\ m/s$ in previous chapter. The flutter speed of a wing that is composed of three identical segments is lower than a wing that is composed of three segments where the parameters of each segment are different from each other and decreases from root to tip.

5.1.7 Goland wing at 50% span extension

In this section, the flutter behavior of variable-span morphing wing is analyzed. The Goland wing parameters (listed in Table 4.1) are used in this part. The wingspan extends by 50%, thus the semi-span length becomes 9.144 m. The findings are compared with the study conducted by Ajaj et al. [60]. A top view of the variable-span morphing wing is illustrated in Figure 5.11.

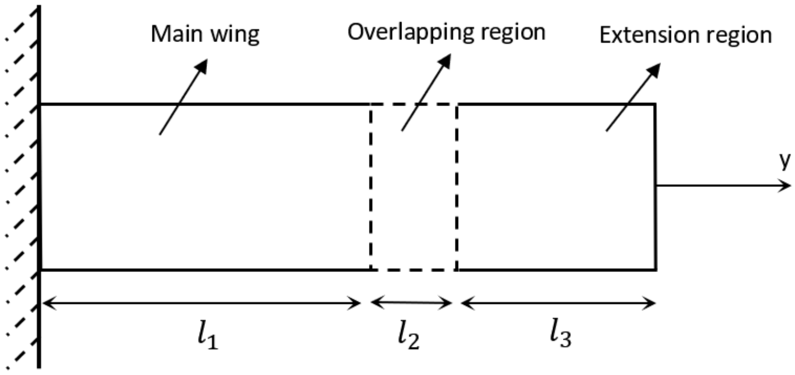

Figure 5.11 : Top view of variable-span morphing wing.

In this configuration, chord lengths of segments are assumed to be equal to each other. For 50% extended Goland wing, first segment is the main wing, second segment is the overlapping region and third segment is the extension region. The length of first segment is $L_1 = 5\ m$, second segment is $L_2 = 1.096\ m$ and third segment is $3.048\ m$. Variation of speed with damping for Goland wing at 50% extension is given in Figure 5.12.

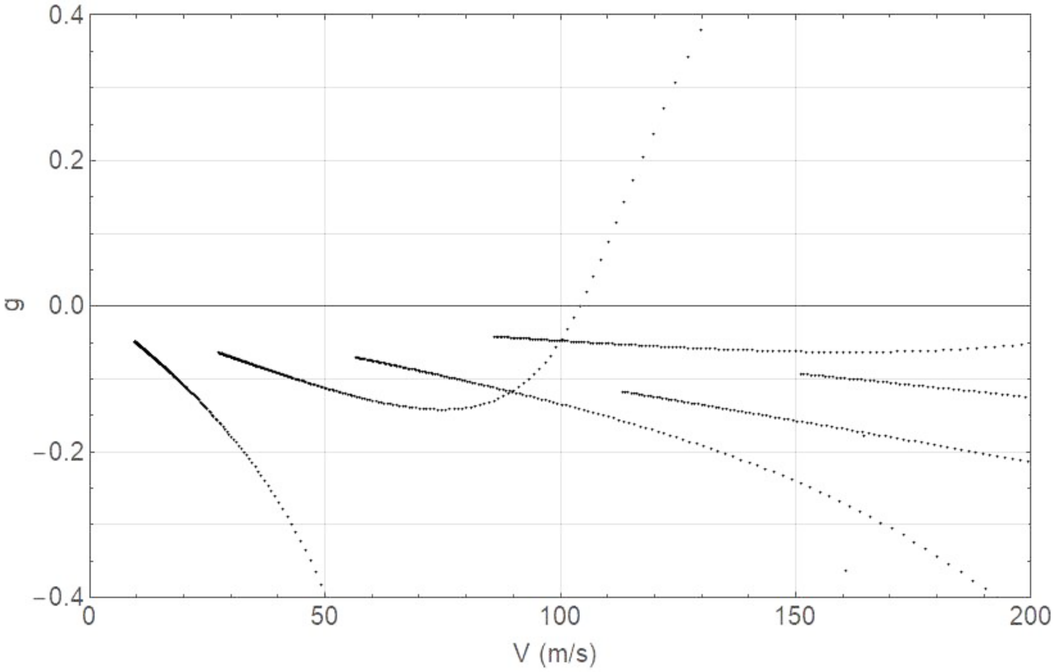

Figure 5.12 : Variation of speed with damping for Goland wing at 50% extension.

Ajaj et al. [60] reported the flutter speed of Goland wing at 50% extension is at around $100\ m/s$. In the current study, the flutter speed is found as $104.1\ m/s$ with the error 3.93 %. The flutter speed of Goland wing was found as $136.10\ m/s$ in Chapter 4. Taken together, these findings show that flutter speed decreases as the wing span extends. The variation of frequency with damping and the variation of speed with frequency for Goland wing at $50\ \%$ extension are given in Figure 5.13 and Figure 5.14, respectively.

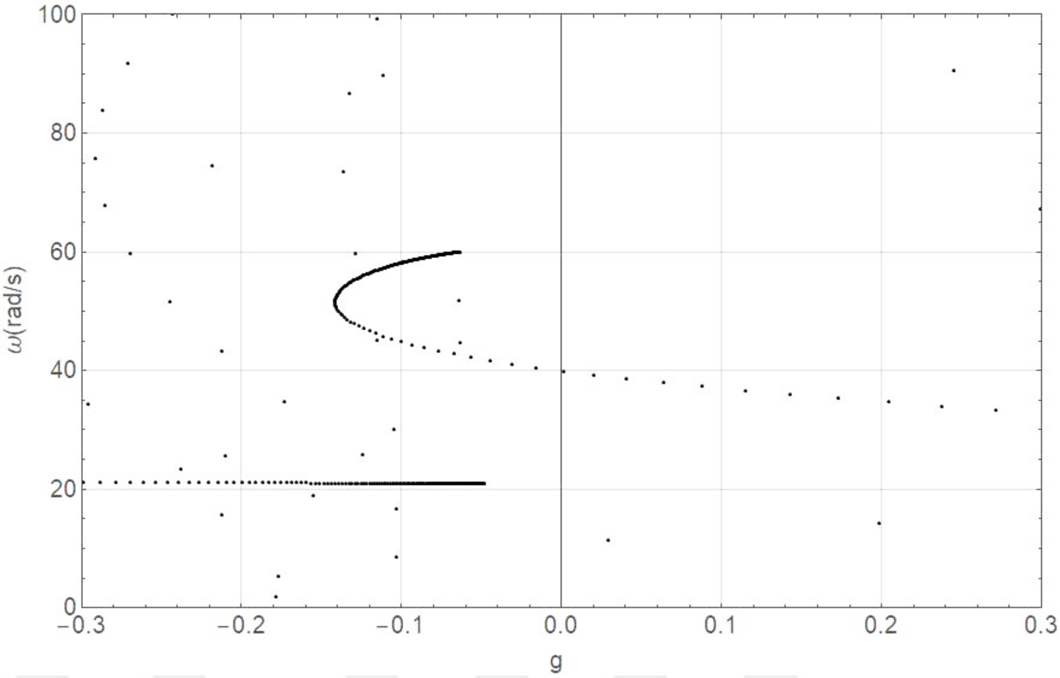

Figure 5.13 : Variation of frequency with damping for Goland wing at 50% extension.

The flutter frequency is found as $39.9\ rad/s$ at a point where g takes a value 0. At one-segment Goland wing model, the flutter frequency was found to be $70.01\ rad/s$. As is the case with the flutter speed, the flutter frequency also decreases as wing span extends.

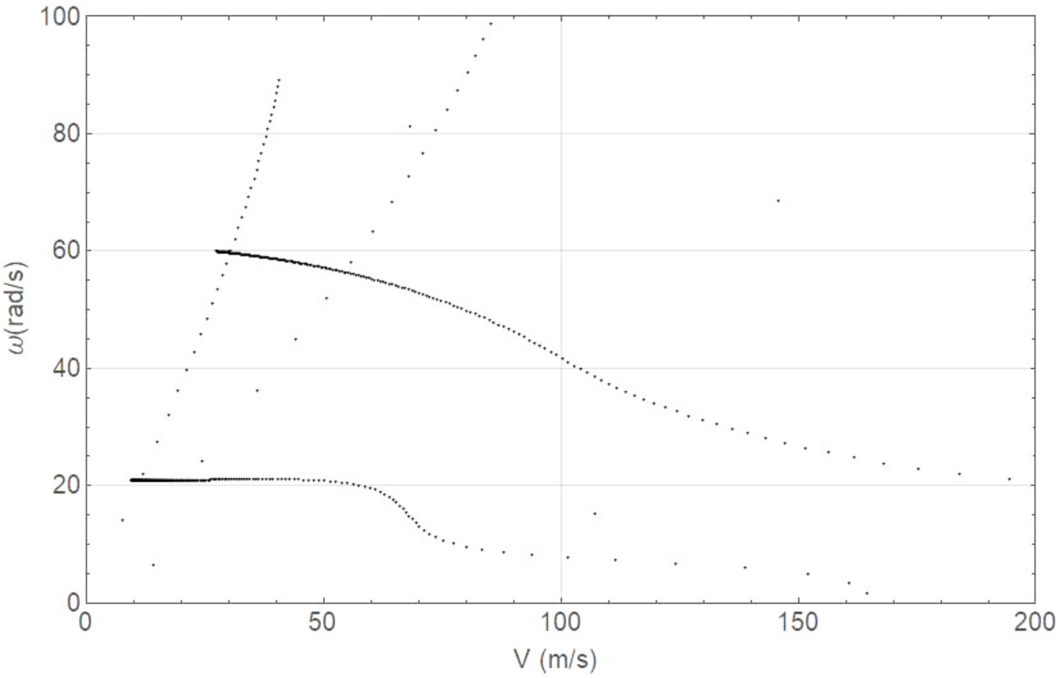

Figure 5.14 : Variation of speed with frequency Goland wing at 50% extension.

The flutter values of 50% extended and 0% extended wing are also given in a compact form. The flutter speed and frequency are compared for both two configurations in Table 5.12.

Table 5.12 : The comparison of flutter values of Goland wing at 50% and 0% span extension.

Critical values for flutter	50% extension	0% extension
Flutter Speed, m/s	104.1	136.10
Flutter Frequency, rad/s	39.9	70.01

After validating the flutter characteristics of Goland wing at $50\ \%$ span extension, the natural frequencies are also analyzed. The first six natural frequencies of Goland wing at $50\ \%$ span extension are compared with natural frequencies of Goland wing without any extension in Table 5.13.

Table 5.13 : The comparison of first six natural frequencies of Goland wing at 50% span extension.

	Frequency	
Mode number	50% extension	0% extension
1	21.74	49.58
2	62.64	97.28
3	130.36	248.59
4	194.76	356.33
5	283.18	451.90
6	372.23	610.00

As can be seen from Table 5.13, the natural frequencies for each mode decreases dramatically when span extends by 50%.

5.1.8 HALE wing at 50% span extension

The HALE wing at 50% span extension is also analyzed after validating flutter values of Goland wing at 50% span extension. The lengths of first and second segment are assigned by author. The length of first segment is taken as $13.333\ m$ whilst the length of second segment is taken as $2.667\ m$. Thus, the length of third segment of the HALE wing is taken as $8\ m$. Table 5.14 compares the first six natural frequencies of HALE wing at 50% span extension with natural frequencies of HALE wing at 0% extension for each mode.

Table 5.14 : The comparison of first six natural frequencies of HALE wing at 50% span extension.

	Frequency	
Mode number	50% extension	0% extension
1	0.99	2.24
2	6.25	14.06
3	17.47	31.05
4	20.70	39.36
5	27.43	77.12
6	56.79	93.14

It is apparent from Table 5.14 that the natural frequencies of each mode decreases significantly when the wing span extends by 50%. The variation of the speed with damping of HALE wing at 50% extension is given in Figure 5.15.

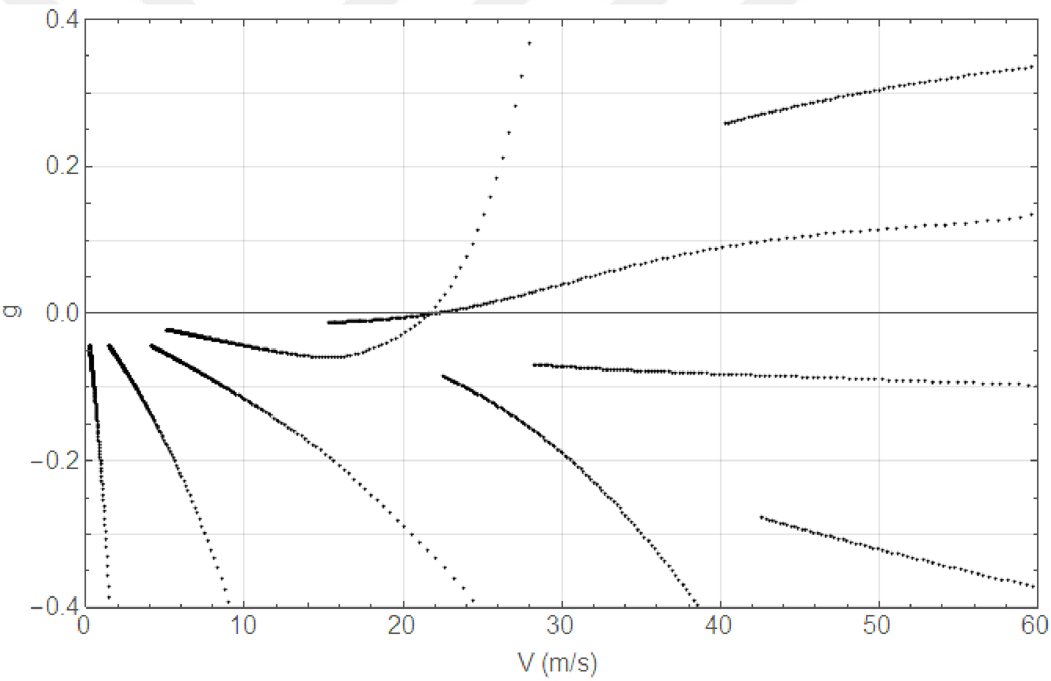

Figure 5.15 : Variation of speed with damping for HALE wing at 50% extension.

The flutter speed of the HALE wing without extension was found in previous chapter as 32.22 m/s. As the wing span of HALE wing extends by 50%, the flutter speed decreases to 21.47 m/s. The variation of frequency with damping of HALE wing at 50% extension is given in Figure 5.16.

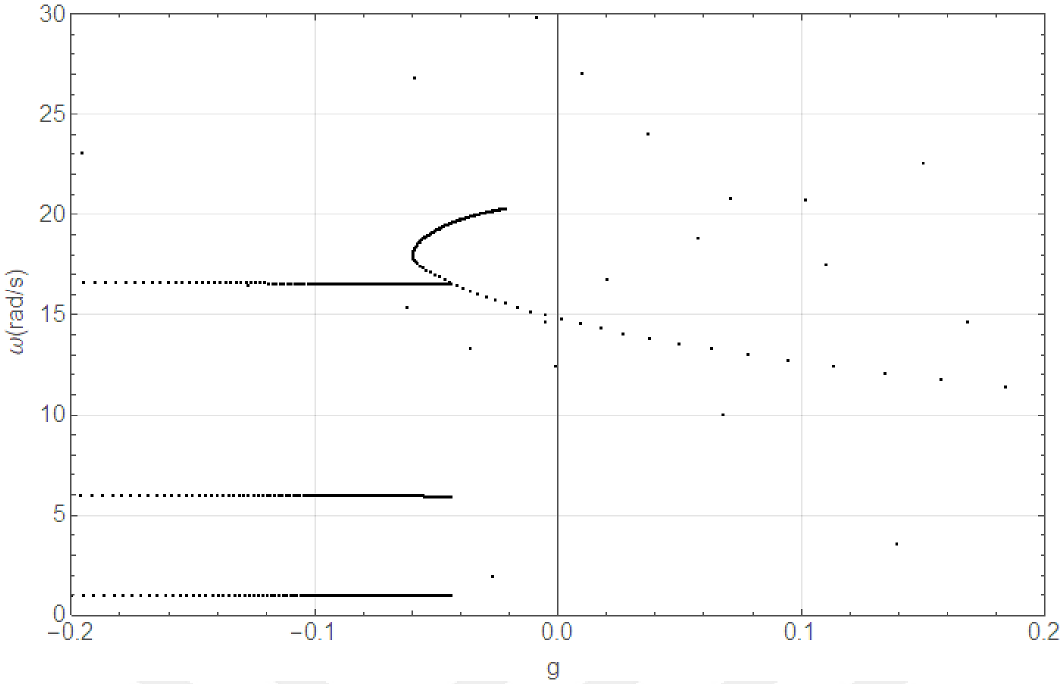

Figure 5.16 : Variation of frequency with damping for Goland wing at 50% extension.

The flutter frequency of HALE wing without extension was found as 22.39 rad/s. As can be seen from Figure 5.16 that the flutter frequency is found as 14.75 rad/s at 50% extension. The comparison of flutter values of HALE wing at 50% extension with the 0% extension configuration is given in Table 5.15.

Table 5.15 : The comparison of flutter values for Goland wing at 50% and 0% span extension.

Critical values for flutter	50% extension	0% extension
Flutter Speed, m/s	21.47	32.22
Flutter Frequency, rad/s	14.75	22.39

It can be easily seen from Table 5.15 that the flutter speed and frequency are decrease dramaticaly as expected when the wing span extends by 50%.

5.2 Effect of Span-Morphing Mechanism on Flutter Characteristics

Morphing wing mechanism considerably effects the flutter behavior of air vehicles by changing its geometrical shape. Span morphing concept brings many advantages to aircrafts such as long endurance flight, roll control, better maneuverability, fuel saving etc. However, change in wing span length may cause some dynamic instabilities. In this section, natural frequency, flutter speed and flutter frequency characteristics are analyzed for variable-span morphing wing.

5.2.1 Effect of span morphing mechanism on natural frequency

The natural frequency of Goland wing is investigated for different span extensions. The second mode is chosen as the basis for this case. The variation of natural frequency with span extension is given in Figure 5.17.

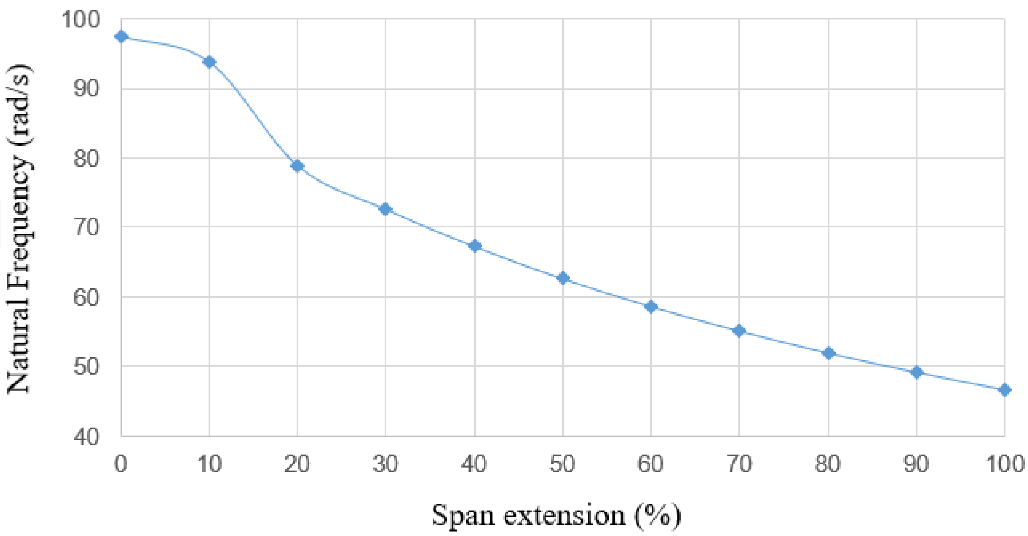

Figure 5.17 : Variation of natural frequency of second mode with span morphing extension for Goland wing.

From Figure 5.17, 0% extension represents the fully retracted wing configuration whilst 100% represents the fully extended wing configuration. It is considered only the third segment extends along the spanwise. The span lengths of second and third segments are unchanged which are $L_1 = 5\ m$ and $L_2 = 1.096\ m$. There is an important difference in terms of natural frequency between fully rectracted and fully extended wing configurations. The natural frequency of second mode was obtained as 97.58 rad/s at 0% extension of Goland wing. It can be seen from Figure 5.17 that the natural frequency of second mode is found as 46.67 rad/s at 100% extension. These findings indicates a significant decrease in natural frequency between 0% extension and 100% extension of Goland wing.

5.2.2 Effect of span morphing mechanism on flutter speed

The flutter speed is analyzed for span extension of Goland wing in various percentages. The wing tends to show dynamic instabilities in higher aspect ratio. Due to this reason, investigation of flutter behavior is crucial for the telescopic span morphing wings. The flutter speed is analyzed for different elongation ratios of wing. The variation of flutter speed with span morphing extension is given in Figure 5.18.

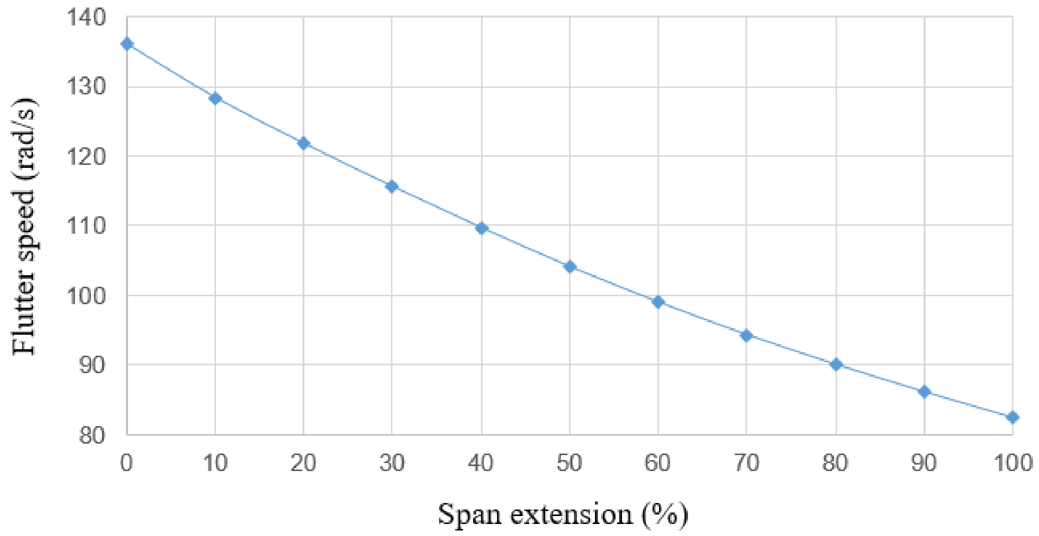

Figure 5.18 : Variation of flutter speed with span morphing extension for Goland wing.

As Figure 5.18 presents, there is a significant difference in flutter speed between fully retracted and fully extended wing configurations. When the wing extends its span length by 100%, the flutter speed decreases to 82.4 m/s. It is apparent that flutter speed decreases dramatically as wing span extends.

Another important finding is that the flutter speed reduction relatively high at the initial stages of the wing span extension. As wing span extends by 10%, the difference between the flutter speed for both configurations is found as 7.7 m/s. On the other hand, the difference between flutter speed is observed as 3.7 m/s when wing span extends from 90% to 100%. From these observations, it can be seen that the reduction in flutter speed is higher in earlier stages of morphing process.

5.2.3 Effect of span morphing mechanism on flutter frequency

The variable-span morphing wing mechanism also considerably effects the flutter frequency. The flutter frequencies are obtained for different elongation ratios of the wing span. The variation of flutter frequency with wing span extension is given in Figure 5.19.

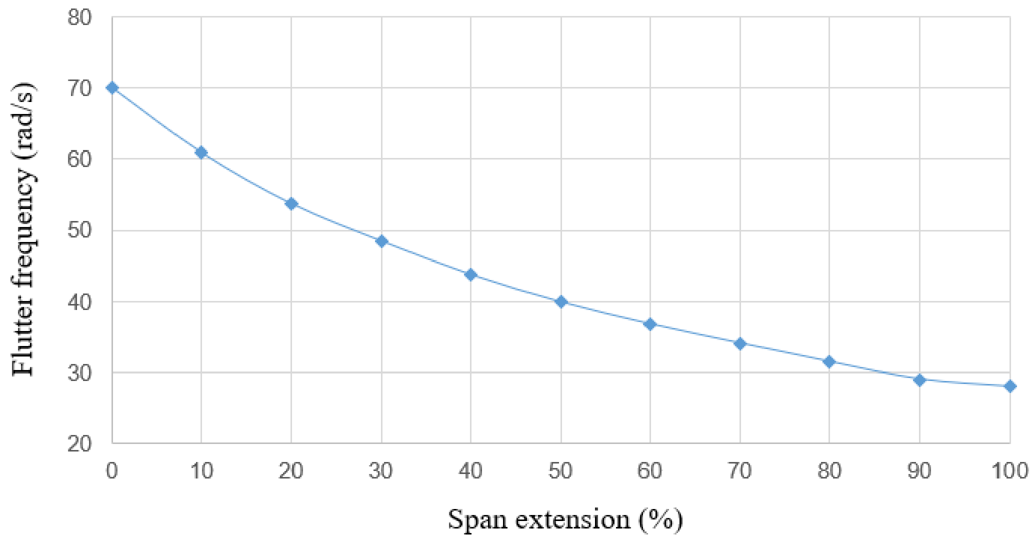

Figure 5.19 : Variation of flutter frequency with span morphing extension for Goland wing.

The wing prones to show dynamic instabilities as wing span length elongates through the spanwise. From the Figure 5.19 it can be seen that the flutter frequency also dramatically decreases as wing span length extends, which is an expected outcome. As the wing span is morphed from fully retracted configuration to fully extended configuration, the flutter frequency decreases from $70.01\ rad/s$ to $28.05\ rad/s$. It can be also deduced that the reduction in flutter frequency is relatively high in the early stages of morphing. The reduction in flutter frequency between 0% wing extension and 10% wing extension is observed as $9.16\ rad/s$. Additionally, the reduction in flutter frequency between 90% wing extension and 100% wing extension is found as $1.02\ rad/s$.

6. CONCLUSION AND DISCUSSIONS

6.1 Concluding Remarks

The aim of this thesis is to analyze the flutter characteristics of a variable-span morphing wing oscillating in pitch and plunge motions under subsonic flight conditions. The morphing wing concept has gained a great deal of attention in recent years. The span morphing concept, which is investigated in this thesis, has ability to change wingspan along spanwise. By variable-span morphing mechanism, a better flight efficiency and aircraft maneuverability can be obtained alongside fuel efficieny and noise reduction. However, this technology may cause to some dynamic instabilities such as flutter or LCOs. Therefore, the aerodynamic, structural, aeroelastic and control characteristics of span morphing aircraft should be analyzed in detail. One of the major aims of this thesis is to contribute to the knowledge in this field by analyzing the aeroelastic behavior of variable-span morphing wings.

Prior to determining the flutter behavior of telescopic span morphing wing, the conventional wing is analyzed in detail. The unswept cantilevered wing is modeled as an Euler-Bernoulli beam which is widely preferred to simplify the wing structural model. Aerodynamic loads acting on the wing are represented by the Theodorsen's aerodynamic theory. The differential equations of motion for free vibration and aeroelastic flutter are derived by the Hamilton's principle. As a solution method, the DTM is implemented to these differential equations of motion and associated boundary conditions. In order to achieve natural frequencies and aeroelastic characteristics of an cantilevered aircraft wing, the classsical frequency domain solution k-method is employed.

To validate the accuracy and reliability of the developed algorithm, two wing types, Goland wing and HALE wing that are well-known in literature are taken into consideration. The case studies are performed to obtain natural frequencies, flutter velocity and flutter frequency of Goland and HALE wings. The findings of case studies are presented as quantitatively and qualitatively for both two wing models. By comparing current findings to those of older investigations, it should be emphasized that the results from DTM have very high precision.

The three-stepped Euler-Bernoulli beam model is used for the flutter analysis of variable-span morphing wing. Goland and HALE wings are also used as the basis for these analyses. All of the parameters except the half span length for each segment are taken exactly the same with the original parameter of Goland and HALE wings. Numerous validation cases are performed to ensure that the stepped beam model works well. By three-stepped beam model, natural frequency, the flutter speed and frequency values were obtained as the same with one-segment (without extension) Goland and HALE wings.

Another case study is the analysis of three-stepped Goland wing with three different segments. The parameters of second segment are taken as two-third of the first segment where the parameters of third segment are taken as one-third of the first segment. The flutter speed of a wing that is composed of three identical segments is lower than a wing that is composed of three segments where the parameters of each segment are different from each other and decreases from root to tip.

The variable-span morphing wing at 50% span extension is also investigated by using three-stepped beam model. The flutter speed and frequency values of 50% extended Goland wing are compared with data from literature. The comparison showed that there is an excellent agreement between findings. The flutter speed and frequency values decrease dramatically when the wing extends its span by 50%. The current findings highlight the importance of flutter analysis of variable span morphing wings.

The natural frequency and flutter characteristics of variable-span morphing wing is analyzed for different elongation ratios of wing. It is assumed that only the third segment extends its span where the span lengths of first and second segment are constant in all cases. It is observed that there is a significant difference in natural frequencies, flutter speed and flutter frequency values between fully retracted and fully extended wing configurations. The natural frequency, flutter speed and flutter frequency decrease substantially when the wing is fully extended. The findings of this study support the idea that flutter values decrease as wing span increases.

Another important finding is that the natural frequency, flutter speed and flutter frequency reduction are relatively high at the initial stages of the wing span extension, which is an expected outcome. These results have significant implications for understanding of how span extension affects the flutter behavior of aircraft. From these several analyses of telescopic span morphing wing, it can be concluded that the aeroelastic analysis has a vital role for morphing wing concept.

6.2 Recommendations for Future Work

In this thesis, the chord lengths of each segment were assumed as constant. As a future work, the study may be repeated using three-stepped beam model with different chord lengths for each segment. The effects of chord length of each segment to flutter characteristics may be investigated. Another possible investigation may be conducting the analysis of the flutter behavior of variable span morphing wing with changing the structural beam model such as Timoshenko beam.

REFERENCES

[1] Matter, Y. S., Darabseh, T. T., and Mourad, A. H. I. (2018). Flutter analysis of a viscoelastic tapered wing under bending–torsion loading, *Meccanica, 53*(15), 3673-3691.

[2] Collar, A. R. (1946). The Expanding Domain of Aeroelasticity, *Journal of the Royal Aeronautical Society, 1,* pp. 613-636.

[3] Bisplinghoff, R. L., Ashley, H., and Halfman, R. L. (1955). *Aeroelasticity*. Dover Publications Inc., New York.

[4] Pacheco, D. R., Marques, F. D., & Ferreira, A. J. (2018). Finite element analysis of fluttering plates reinforced by flexible beams: An energy-based approach, *Journal of Sound and Vibration, 435,* 135-148.

[5] Amato, E. M., Polsinelli, C., Cestino, E., Frulla, G., Joseph, N., Carrese, R., & Marzocca, P. (2019). HALE wing experiments and computational models to predict nonlinear flutter and dynamic response, *The Aeronautical Journal, 123*(1264), 912-946.

[6] Hassanalian, M., Quintana, A., and Abdelkefi, A. (2018). Morphing and growing micro unmanned air vehicle: Sizing process and stability. *Aerospace Science and Technology, 78,* 130-146.

[7] Zi, K. A. N., Daochun, L. I., XIANG, J., and CHENG, C. (2020). Delaying stall of morphing wing by periodic trailing-edge deflection. *Chinese Journal of Aeronautics, 33*(2), 493-500.

[8] Dimino, I., Lecce, L., and Pecora, R. (2017). *Morphing Wing Technologies: Large Commercial Aircraft and Civil Helicopters.* Butterworth-Heinemann.

[9] Li, D., Zhao, S., Da Ronch, A., Xiang, J., Drofelnik, J., Li, Y., and Rudenko, A. (2018). A review of modelling and analysis of morphing wings. *Progress in Aerospace Sciences, 100,* 46-62.

[10] **Hussain, S. A.** (2017). Review of Morphing Wing. (Master's Thesis). Retrieved from *https://www.researchgate.net/publication/328655295_Review_of_Morphing_Wing*

[11] **Kehoe, M. W.** (1995). *A Historical Overview of Flight Flutter Testing,* NASA Technical Memorandum 4720.

[12] **Collar, A. R.** (1978). The first fifty years of aeroelasticity. *Aerospace (Royal Aeronautical Society Journal), 5*(2), 12-20.

[13] **Garrick, I. E., and Reed III, W. H.** (1981). Historical development of aircraft flutter. *Journal of Aircraft, 18*(11), 897-912.

[14] **Tolve, L. A. (1958).** History of flight flutter testing. *Flight Flutter Testing Symposium, NASA SP-385*, 159-166.

[15] **NACA Subcommittee.** (1964). A survey and evaluation of flutter research and engineering. Technical Report 56112, NACA.

[16] **BORST, R., and STROME, R.** (1992). E-6 flutter investigation and experience. In *Astrodynamics Conference*, 4601.

[17] **Zhao, X., Cao, C., and Guo, P.** (2018). Simulation analysis study on the flutter characteristics of control rudder in high speed flight vehicle. *In Journal of Physics: Conference Series*, *1053*(1), 012056. IOP Publishing.

[18] **Url-1** *<https://fighterjetsworld.com/air/the-story-of-a-lucky-f-117a-pilot-who-survived-nighthawk-disintegration-at-the-chesapeake-air-show/13994/>*, data retrieved 29.01.2020.

[19] **Luber, W. G.** Structural Dynamic and Flutter Testing. NATO.

[20] **Frazer, R.A., Duncan W.J. and Collar A.R.** (1946). *Elementary Matrices.* Macmillan, New York.

[21] **Broadbent, E. G.** (1956). Aeroelastic Problems in connection with High-Speed Flight. *The Aeronautical Journal*, *60*(547), 459-475.

[22] **BALDOCK, J., and Skingle, C.** (1973). Flutter technology in the United Kingdom-A survey. *In Dynamics Specialists Conference*, 330.

[23] **Mazet, R.** (1968). AGARD Manual on Aeroelasticity, *6*.

[24] **Goland, M.** (1945). The flutter of a uniform cantilever wing, *Journal of Applied Mechanics*, *12*(4), A197–A208.

[25] **Goland, M., and Luke, Y. L.** (1948). The flutter of a uniform wing with tip weights. *Journal of Applied Mechanics, 15*(1), 13-20.

[26] Runyan, H. L., and Sewall, J. L. (1948). Experimental investigation of the effects of concentrated weights on flutter characteristics of a straight cantilever wing. Technical Report 1594, NACA.

[27] Theodorsen, T. (1934). General theory of aerodynamic instability and the mechanism of flutter. Technical Report 496, NACA, 413-433.

[28] Gu, Y., and Yang, Z. (2012). Modified pk method for flutter solution with damping iteration. *AIAA journal, 50*(2), 507-510.

[29] Hodges, D. H., and Pierce, G. A. (2011). *Introduction to structural dynamics and aeroelasticity, 15*. Cambridge University Press.

[30] Fung, Y.C. 1993. *An Introduction to the Theory of Aeroelasticity*. Dover Publications, New York.

[31] Patil, M. J., Hodges, D. H., and Cesnik, C. E. (2001). Nonlinear aeroelasticity and flight dynamics of high-altitude long-endurance aircraft. *Journal of Aircraft, 38*(1), 88-94.

[32] Mardanpour, P., and Hodges, D. H. (2015). On the importance of nonlinear aeroelasticity and energy efficiency in design of flying wing aircraft. *Advances in Aerospace Engineering.*

[33] Patil, M. J., Hodges, D. H., and Cesnik, C. E. (2000). Nonlinear aeroelastic analysis of complete aircraft in subsonic flow. *Journal of Aircraft*, *37*(5), 753-760.

[34] Richards, P. W., Yao, Y., Herd, R. A., Hodges, D. H., and Mardanpour, P. (2016). Effect of inertial and constitutive properties on body-freedom flutter for flying wings. *Journal of Aircraft*, *53*(3), 756-767.

[35] Tang, D., and Dowell, E. H. (2001). Experimental and theoretical study on aeroelastic response of high-aspect-ratio wings. *AIAA journal*, *39*(8), 1430-1441.

[36] Moosavi, M. R., Oskouei, A. N., and Khelil, A. (2005). Flutter of subsonic wing. *Thin-walled structures*, *43*(4), 617-627.

[37] Weishuang, L. U., Yun, T. I. A. N., and Peiqing, L. I. U. (2017). Aerodynamic optimization and mechanism design of flexible variable camber trailing-edge flap. *Chinese Journal of Aeronautics*, *30*(3), 988-1003.

[38] Ippolito, C., Nguyen, N., Totah, J., Trinh, K., and Ting, E. (2013). Initial assessment of a variable-camber continuous trailing-edge flap system on a rigid wing for drag reduction in subsonic cruise. *AIAA Guidance, Navigation, and Control and Co-located Conferences, Boston*, 19-22.

[39] Blondeau, J., and Pines, D. (2004). Pneumatic morphing aspect ratio wing. *In 45th AIAA/ASME/ASCE/AHS/ASC Structures, Structural Dynamics & Materials Conference*, 1808.

[40] Ivanco, T., Scott, R., Love, M., Zink, S., and Weisshaar, T. (2007). Validation of the Lockheed Martin morphing concept with wind tunnel testing. *In 48th AIAA/ASME/ASCE/AHS/ASC Structures, Structural Dynamics, and Materials Conference*, 2235.

[41] Weisshaar, T. A. Morphing Aircraft Technology–New Shapes for Aircraft Design. NATO documents unclassified. *In Meeting Proceedings RTO-MP-AVT-141.*

[42] Henry, J., and Pines, D. (2007). A mathematical model for roll dynamics by use of a morphing-span wing. *In 48th AIAA/ASME/ASCE/AHS/ASC Structures, Structural Dynamics, and Materials Conference*, 1708.

[43] Seigler, T. M., Bae, J. S., and Inman, D. J. (2004). Flight control of a variable span cruise missile. *In ASME International Mechanical Engineering Congress and Exposition, 47063*, 565-574).

[44] Ajaj, R., Friswell, M., Saavedra Flores, E., Little, O., and Isikveren, A. (2012). Span morphing: a conceptual design study. *In 53rd AIAA/ASME/ASCE/AHS/ASC Structures, Structural Dynamics and Materials Conference*, 1510.

[45] Li, D., Guo, S., He, Y., and Xiang, J. (2012). Nonlinear aeroelastic analysis of a morphing flap. *International Journal of Bifurcation and Chaos*, *22*(05), 1250099.

[46] Huang, C., Yang, C., Wu, Z., and Tang, C. (2018). Variations of flutter mechanism of a span-morphing wing involving rigid-body motions. *Chinese Journal of Aeronautics, 31*(3), 490-497.

[47] Huang, R., and Qiu, Z. (2013). Transient aeroelastic responses and flutter analysis of a variable-span wing during the morphing process. *Chinese Journal of Aeronautics, 26*(6), 1430-1438.

[48] Bauchau, O. A., and Craig, J. I. (2009). *Euler-Bernoulli beam theory*. In Structural analysis. 173-22. Springer, Dordrecht.

[49] **Runyan, H. L., and Watkins, C. E.** (1950). Flutter of a uniform wing with an arbitrarily placed mass according to a differential equation analysis and a comparison with experiment. Technical Report 1848, NACA.

[50] **Kaya, M. O., and Ozgumus, O. O.** (2007). Flexural–torsional-coupled vibration analysis of axially loaded closed-section composite Timoshenko beam by using DTM. *Journal of Sound and Vibration*, *306*(3-5), 495-506

[51] **Yalcin, H. S., Arikoglu, A., and Ozkol, I.** (2009). Free vibration analysis of circular plates by differential transformation method. *Applied Mathematics and Computation, 212*(2), 377-386.

[52] **Kim, T.** (2016). Parametric model reduction for aeroelastic systems: Invariant aeroelastic modes. *Journal of Fluids and Structures, 65*, 196-216.

[53] **Eslimy-Isfahany, S. H. R., Banerjee, J. R., and Sobey, A. J.** (1996). Response of a bending–torsion coupled beam to deterministic and random loads. *Journal of Sound and Vibration*, *195*(2), 267-283.

[54] **Hashemi, S. M., and Richard, M. J.** (2000). A Dynamic Finite Element (DFE) method for free vibrations of bending-torsion coupled beams. *Aerospace Science and Technology*, *4*(1), 41-55.

[55] **Goraj, Z., Frydrychewicz, A., Świtkiewicz, R., Hernik, B., Gadomski, J., Goetzendorf-Grabowski, T., and Chajec, W.** (2004). High altitude long endurance unmanned aerial vehicle of a new generation–a design challenge for a low cost, reliable and high performance aircraft. *Buletin of the Polish Academy of Sciences Technical Sciences*, *52*(3).

[56] **Arena, A., Lacarbonara, W., and Marzocca, P.** (2013). Nonlinear aeroelastic formulation and postflutter analysis of flexible high-aspect-ratio wings. *Journal of aircraft, 50*(6), 1748-1764.

[57] **Tarabi, A., Ghasemloo, S., and Mani, M.** (2016). Experimental investigation of a variable-span morphing wing model for an unmanned aerial vehicle. *Journal of the Brazilian Society of Mechanical Sciences and Engineering, 38*(7), 1833-1841.

[58] **Lee, D. H., and Weisshaar, T.** (2005). Aeroelastic studies on a folding wing configuration. *In 46th AIAA/ASME/ASCE/AHS/ASC Structures, Structural Dynamics and Materials Conference,* 1996.

[59] Hashemi, S. M., and Richard, M. J. (2000). A Dynamic Finite Element (DFE) method for free vibrations of bending-torsion coupled beams. *Aerospace Science and Technology*, *4*(1), 41-55.

[60] Ajaj, R. M., Omar, F. K., Darabseh, T. T., and Cooper, J. (2019). Flutter of Telescopic Span Morphing Wings. *International Journal of Structural Stability and Dynamics*, *19*(06), 1950061.

CURRICULUM VITAE

Name Surname : Damla DURMUŞ

Place and Date of Birth : 03.07.1993

E-Mail : durmus17@itu.edu.tr

EDUCATION:

- **B.Sc.:** 2017, University of Turkish Aeronautical Association, Faculty of Aeronautics and Astronautics, Aeronautical Engineering Department
- **M.Sc.:** 2020, Istanbul Technical University, Department of Aeronautical and Astronautical Engineering, Aeronautical and Astronautical Engineering Program

PROFESSIONAL EXPERIENCE AND REWARDS:

- 2018-Present: Research Assistant, Istanbul Technical University, Department of Aeronautical Engineering

PUBLICATIONS, PRESENTATIONS AND PATENTS ON THE THESIS:

- Durmus D., M. O. Kaya. Ses Altı Uçuş Koşullarındaki Bir Uçak Kanadının Diferansiyel Dönüşüm Yöntemi ile Çırpınma Analizi. 8. Ulusal Havacılık ve Uzay Konferansı, THKÜ, 9-11 Eylül 2020, Ankara.